Automatica 164 (2024) 111621

Contents lists available at ScienceDirect

Automatica

journal homepage: www.elsevier.com/locate/automatica

A dynamic controller synthesis methodology for negative imaginary systems using the internal model control principle☆

Parijat Bhowmick [a,*], Suleiman Kurawa [b], Somasundar Kannan [c], Alexander Lanzon [b]

[a] Department of EEE, IIT Guwahati, Assam 781039, India
[b] Control Systems Centre, Department of EEE, University of Manchester, Manchester M13 9PL, UK
[c] Department of EE, Robert Gordon University, Aberdeen, Scotland, United Kingdom

ARTICLE INFO

Article history:
Received 12 July 2021
Received in revised form 27 September 2023
Accepted 22 February 2024
Available online xxxx

Keywords:
Negative imaginary systems
Vibration control
DC-gain
Positive feedback
Internal model control
LMIs
Dynamic controller synthesis

ABSTRACT

This paper proposes a new controller design methodology for stable and minimum-phase Negative Imaginary (NI) systems relying on the classical Internal Model Control (IMC) principle. The closed-loop stability of the proposed scheme depends only on the DC loop gain, which is theoretically justified by the feedback stability results of the NI theory. The main objective is to design the Youla parameter of an IMC scheme, which has been cast as a Negative Imaginary (NI) controller synthesis problem. Two different methodologies have been proposed. A frequency-domain IMC design approach is first presented, which depends on solving a constrained, linear, least-square estimation problem. Then, an LMI-based methodology is developed, which can be solved by the commercially available SDP solver packages. An in-depth simulation case study on the vibration attenuation problem of a lightweight cantilever beam (a potential application of the NI theory) was carried out to demonstrate the usefulness of the NI-based IMC design methodology. Finally, the simulation results were experimentally validated on a custom-made vibration suppressor to confirm the feasibility of the proposed scheme.

1. Introduction

Negative Imaginary (NI) systems theory has flourished as a stand-alone robust stability analysis and controller synthesis framework over the past fifteen years since its inception in 2008 (Lanzon & Petersen, 2008). In the simplest sense, a system is called NI (resp. SNI) if the imaginary part of the system's transfer function remains non-positive (resp. negative) for all $\omega \in (0, \infty)$. NI systems property is closely related to counter-clockwise input–output dynamics in a nonlinear setting (Angeli, 2006) and a class of dissipative systems defined with respect to the system's input and the time-derivative of the system's output (Bhowmick & Lanzon, 2019, 2020, 2024; Bhowmick & Patra, 2017; Lanzon & Bhowmick, 2023). NI systems theory offers a simple closed-loop stability condition that depends only on the DC loop gain information $[\lambda_{\max}[H(0)G(0)] < 1$ w.r.t. Fig. 3] and hence, the theory can be easily applied to practical systems for which an exact mathematical model is unavailable (Lanzon & Petersen, 2008; Petersen, 2016; Xiong, Petersen, & Lanzon, 2010). NI theory finds potential applications in vibration control of highly-resonant flexible structures (Lanzon & Petersen, 2008), robotic manipulators (Mabrok, Kallapur, Petersen, & Lanzon, 2014), in nano-positioning applications (Nikooienejad & Reza Moheimani, 2022), in train platooning (Li, Wang, Shan, Lanzon, & Petersen, 2021), in cooperative control of a variety of multi-agent systems (Hu, Lennox, & Arvin, 2022; Shi, Petersen, & Vladimirov, 2023; Su, Bhowmick, & Lanzon, 2023a, 2023b, 2023c; Tran, Garratt, & Petersen, 2021), etc. Recently, NI theory has been extended to improper and non-rational systems (Ferrante, Lanzon, & Ntogramatzidis, 2016; Ferrante & Ntogramatzidis, 2013) and also to discrete-time LTI systems (Ferrante, Lanzon, & Ntogramatzidis, 2017; Liu & Xiong, 2017).

NI literature has been enriched by many significant findings on NI controller synthesis. The articles (Dey, Patra, & Sen, 2019; Song, Lanzon, Patra, & Petersen, 2012a; Xiong, Lam, & Petersen, 2016) laid significant contributions in designing static state feedback and static output feedback controllers utilising the NI framework. Song, Lanzon, Patra, and Petersen (2010, 2012b) took the first step to propose a dynamic stable-NI controller synthesis

☆ This work was supported by the Engineering and Physical Sciences Research Council (EPSRC) [grant number EP/R008876/1] and the Science and Engineering Research Board (SERB), DST, India [grant number SRG/2022/000892]. All research data supporting this publication are directly available within this publication. For the purpose of open access, the authors have applied a Creative Commons Attribution (CC BY) licence to any Author Accepted Manuscript version arising. The material in this paper was not presented at any conference. This paper was recommended for publication in revised form by Associate Editor James Lam under the direction of Editor Florian Dorfler.

* Corresponding author.
E-mail addresses: parijat.bhowmick@iitg.ac.in (P. Bhowmick), Suleiman.Kurawa@postgrad.manchester.ac.uk (S. Kurawa), s.kannan1@rgu.ac.uk (S. Kannan), Alexander.Lanzon@manchester.ac.uk (A. Lanzon).

https://doi.org/10.1016/j.automatica.2024.111621
0005-1098/

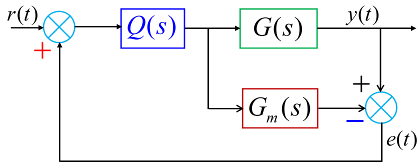

Fig. 1. Block diagram of the classical IMC scheme.

Fig. 2. A custom-made vibration suppressor for testing the NI-based IMC synthesis algorithms.

technique that ensured both robust stability and performance relying on a conversion between the Positive Real (PR) and Bounded Real (BR) frameworks. Liu, Ono, Li, and Wu (2017) introduced an LMI-based dynamic output feedback NI controller synthesis methodology by converting the NI uncertainties into the PR domain. Of late, Bhowmick and Patra (2020) and Kurawa, Bhowmick, and Lanzon (2019) solved the dynamic output feedback NI controller synthesis problem exploiting the Strongly Strict NI (SSNI) (Lanzon, Song, Patra, & Petersen, 2011) and α-SNI systems properties, respectively. However, these techniques primarily rely on the four-block modelling scheme introduced in Scherer, Gahinet, and Chilali (1997) and may face difficulties in fitting a practical NI plant into the four-block framework for synthesis purpose. Besides, very few attempts have been taken so far to provide systematic design guidelines for implementing such controllers in practice.

Motivation and objectives: Drawn by the advancements and limitations of the existing NI controller synthesis techniques, this paper utilises the classical Internal Model Control (IMC) (Garcia & Morari, 1982; Morari & Zafiriou, 1989) framework (in Fig. 1) to synthesise a dynamic controller for the class of stable and minimum-phase NI plants. The primary control objective of an IMC scheme is to design a stable $Q(s)$, known as the Youla parameter, such that steady-state tracking is achieved and closed-loop stability is maintained even in the presence of model mismatch [i.e. when $G_m(s) \neq G(s)$]. This paper proposes a positive feedback IMC scheme (refer to Fig. 4) where the controller $C(s) = Q(s)\left[I + G_m(s)Q(s)\right]^{-1}$ is designed to be a stable-NI or SNI system complying with the relative degree of a given NI plant. A frequency-domain approach and a numerically tractable LMI-based technique will be presented for designing the NI-based IMC controller. The frequency-domain approach seeks to solve a constrained, linear, least-square estimation problem, while the LMI-based technique needs to choose a stable polynomial $d(s)$ such that $\frac{1}{d(s)}G_m(s)^{-1}$ becomes strictly proper. We also provide a set of detailed guidelines on how to choose the required polynomial $d(s)$. The LMI-based design technique facilitates an easy implementation of the scheme with the help of Matlab-based SDP solver packages. An in-depth simulation case study is carried out (in Section 4) on the vibration control problem of a lightweight cantilever beam (inspired by a real-world control problem of a vibration suppressor shown in Fig. 2) to show the usefulness of the NI-based IMC scheme. Finally, experimental validation results are also provided in Section 4.4 to demonstrate the feasibility and effectiveness of the scheme in practice.

Contributions: Below, we mention the key contributions and salient features of this work.

- This paper has developed a new internal model controller (IMC) design methodology for stable and minimum-phase NI systems. Unlike most of the literature on NI controller synthesis, this paper does not only propose a synthesis technique but also provides precise design guidelines for practical implementation;
- The LMI-based methodology offers a convenient, systematic and easy-to-implement IMC synthesis technique due to the commercially available (Matlab-based) SDP solver packages;
- Apart from the LMI-based IMC design methodology, a frequency-domain design methodology is also proposed that remains effective for SISO and decoupled MIMO NI plants;
- The paper has validated the NI-based IMC scheme on a custom-made vibration suppressor (shown in Fig. 2), as vibration control is one of the primary application areas of the NI theory. The disturbance rejection capacity of the controller and its robustness to model-mismatch were also tested.

The paper also gives ideas on how to use a Subspace-based system identification process in real time (via Matlab) while enforcing a particular system property.

Notation and symbols: The notations and acronyms are standard throughout. $\mathbb{R}$ and $\mathbb{C}$ denote respectively the sets of all real and all complex numbers. $\mathbb{R}^{m\times n}$ and $\mathbb{C}^{m\times n}$ represent the sets of all real and all complex matrices of dimensions $(m\times n)$. $\Re(\cdot)$ and $\Im(\cdot)$ express the real and the imaginary parts respectively. $A^\top$, A^* and $\bar{A}$ denote the transpose, complex conjugate transpose and complex conjugate of a matrix A. A^{-*} and $A^{-\top}$ represent shorthand for $\left(A^{-1}\right)^*$ and $\left(A^{-1}\right)^\top$ respectively. $\lambda_{\max}(A)$ denotes the maximum eigenvalue of a matrix A having only real eigenvalues. For a real, rational transfer function matrix $M(s)$, $M(j\omega)^* = M(-j\omega)^\top$. $\mathcal{RH}_\infty^{m\times n}$ denotes the set of all real, rational, proper and asymptotically stable transfer function matrices of dimension $(m\times n)$. $\left[\begin{array}{c|c} A & B \\ \hline C & D \end{array}\right]$ gives a state-space realisation of a real, rational, proper transfer function matrix $M(s) = D + C(sI - A)^{-1}B$.

2. Background and problem formulation

In this section, we present essential technical preliminaries which underpin the proofs of the main results of the paper, and the problem formulation.

2.1. Briefs of NI theory

We begin with the definitions of real, rational and proper NI, SNI and SSNI systems.

Definition 1 (*NI System Lanzon & Chen, 2017; Mabrok et al., 2014*). Let $G(s)$ be the real, rational and proper transfer function matrix of a finite-dimensional, square and causal system G. Then, $G(s)$ is said to be NI without poles at the origin if

(i) $G(s)$ has no poles in $\{s \in \mathbb{C} : \Re[s] > 0 \text{ and } s = 0\}$;
(ii) $j[G(j\omega) - G(j\omega)^*] \geq 0$ for all $\omega \in (0,\infty)$ except the values of ω where $s = j\omega$ is a pole of $G(s)$;
(iii) If $s = j\omega_0$ with $\omega_0 \in (0,\infty)$ is a pole of $G(s)$, then it is at most a simple pole and the residue matrix $\lim_{s\to j\omega_0}(s - j\omega_0)jG(s)$ is Hermitian and positive semidefinite.

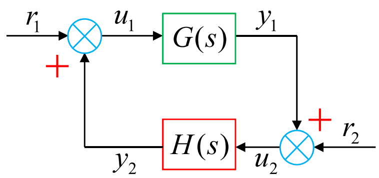

Fig. 3. A positive feedback interconnection of NI systems.

The following lemma, referred to as the NI Lemma, provides a state-space characterisation for NI systems without poles at the origin.

Lemma 1 (*NI Lemma Xiong et al., 2010*). *Let $G(s)$ be the real, rational and proper transfer function matrix of a finite-dimensional, square and causal system G having a minimal state-space realisation $\left[\begin{array}{c|c} A & B \\ \hline C & D \end{array}\right]$. Then, $G(s)$ is NI without poles at the origin if and only if $\det(A) \neq 0$, $D = D^\top$ and there exists a real matrix $Y = Y^\top > 0$ such that*

$$AY + YA^\top \leq 0 \quad \text{and} \quad B + AYC^\top = 0. \tag{1}$$

Definition 2 (*SNI System Lanzon & Petersen, 2008*). Let $G(s)$ be the real, rational and proper transfer function matrix of a finite-dimensional, square and causal system G. Then, $G(s)$ is said to be SNI if $G(s)$ has no poles in $\{s \in \mathbb{C} : \Re[s] \geq 0\}$ and $j[G(j\omega) - G(j\omega)^*] > 0$ for all $\omega \in (0, \infty)$.

Strongly Strict Negative Imaginary (SSNI) systems form a strict subset within the SNI class that satisfy two additional frequency-domain criteria in the neighbourhood of $\omega = 0$ and $\omega = \infty$.

Definition 3 (*SSNI System Lanzon et al., 2011*). Let $G(s)$ be the real, rational and proper transfer function matrix of a finite-dimensional, square and causal system G. Then, $G(s)$ is said to be Strongly Strict Negative Imaginary (SSNI) if

- $G(s)$ is SNI;
- $\lim_{\omega \to 0} j\dfrac{1}{\omega}[G(j\omega) - G(j\omega)^*] > 0$;
- $\lim_{\omega \to \infty} j\omega [G(j\omega) - G(j\omega)^*] > 0$.

Below, we present a slightly modified version of the SSNI lemma (Lanzon et al., 2011) by exploiting (Kurawa et al., 2019, Lemma 2).

Lemma 2 (*SSNI Lemma Kurawa et al., 2019; Lanzon et al., 2011*). *Let $G(s) \in \mathscr{RH}_\infty^{m\times m}$ be the real, rational and proper transfer function matrix of a finite-dimensional, square and causal system G, having a state-space realisation $\left[\begin{array}{c|c} A & B \\ \hline C & D \end{array}\right]$. Suppose $\mathrm{rank}[B] = \mathrm{rank}[C] = m$ and the pair (A, C) is observable. Then, $G(s)$ is SSNI if and only if $D = D^\top$ and there exists a real matrix $Y = Y^\top > 0$ such that $AY + YA^\top < 0$ and $B + AYC^\top = 0$.*

We now recall the closed-loop stability condition for a stable NI system interconnected with an SNI system via positive feedback. Please see Lanzon and Chen (2017) for extended closed-loop stability results of NI-SNI interconnections.

Theorem 1 (*Lanzon & Chen, 2017; Lanzon & Petersen, 2008*). *Let $G(s) \in \mathscr{RH}_\infty^{m\times m}$ be an NI system and $H(s) \in \mathscr{RH}_\infty^{m\times m}$ be an SNI system. Let either $G(\infty) = 0$, or else $G(\infty)H(\infty) = 0$ and $H(\infty) \geq 0$. Then, the positive feedback interconnection of $G(s)$ and $H(s)$ shown in Fig. 3 is asymptotically stable if and only if $\lambda_{\max}[H(0)G(0)] < 1$.*

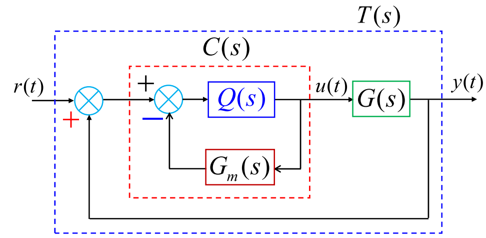

Fig. 4. Equivalent block diagram of the classical IMC scheme shown in Fig. 1.

2.2. IMC principle in brief

The classical IMC scheme has been adopted in this paper from Morari and Zafiriou (1989) and is shown in Fig. 1. An IMC problem seeks to design a stable $Q(s)$, known as the *Youla parameter* (Morari & Zafiriou, 1989), such that the closed-loop scheme shown in Fig. 1 has good nominal performance and remains closed-loop stable even when $G(s) \neq G_m(s)$. Conventionally, an IMC scheme works with negative feedback. However, in this paper, we have considered a positive feedback IMC scheme to fit into the NI framework. The performance of an IMC scheme highly relies on the accuracy of the model $G_m(s)$ of the plant $G(s)$ to be controlled. We do not presume any structure of the model $G_m(s)$ and thus, the model can be obtained via any system identification technique or it can be derived mathematically. For example, we used Matlab system identification toolbox to obtain a model of the plant from the experimental observation [detailed in Section 4].

Fig. 1 can equivalently be drawn as in Fig. 4 where the red-dotted block plays the role of the internal model controller $C(s) = Q(s)[I + G_m(s)Q(s)]^{-1}$.

The Youla parameter is often designed as $Q(s) = G_m(s)^{-1}F(s)$, where $F(s)$ behaves as a low-pass filter to be determined. The filter dynamics significantly influences shaping the steady-state tracking or regulatory response of an IMC scheme.

2.3. Problem formulation

Given a stable and minimum-phase NI (including SNI) plant $G(s)$ and a reasonably accurate model $G_m(s)$ that closely replicates the plant behaviour, design an SNI/SSNI controller $C(s)$ such that the positive feedback IMC scheme shown in Fig. 4 [which is equivalent to Fig. 1] remains asymptotically stable and facilitates a faithful steady-state tracking.

3. Controller design methodologies for stable NI and SNI systems using the IMC principle

This section presents the main theoretical contributions of this paper. Our objective is to develop an internal model control scheme for stable NI or SNI systems relying on the *DC loop gain* condition of NI stability theory (Theorem 1). The proposed idea builds on the classical IMC framework shown in Fig. 4 and offers a frequency-domain and an LMI-based design methodology to synthesise a stabilising NI/SNI/SSNI controller.

3.1. A frequency-domain design approach

Before presenting the frequency-domain design technique for an NI (resp. SNI) controller, we want to recall the standard polynomial factorisation in terms of its even and odd terms. A frequency-domain polynomial $P(s)$ can be factored as

$$P(s) = \underbrace{P_0 + P_2 s^2 + \dots}_{P_{\text{even}}(s^2)} + s\underbrace{(P_1 + P_3 s^2 + \dots)}_{P_{\text{odd}}(s^2)}$$

such that if $P(j\omega) = P_r(\omega) + jP_i(\omega)$, then $P_r(\omega) = P_{\text{even}}(-\omega^2)$ and $P_i(\omega) = \omega P_{\text{odd}}(-\omega^2)$ for all $\omega \in \mathbb{R}$. Using this factorisation, the plant model $G_m(s)$ can be decomposed as $G_m(j\omega) = \dfrac{N_m(j\omega)}{D_m(j\omega)} = \dfrac{N_{mr}(\omega) + jN_{mi}(\omega)}{D_{mr}(\omega) + jD_{mi}(\omega)}$.

Lemma 3 offers a sufficient-type frequency-domain condition for designing a SNI (resp. stable NI) controller $C(s)$ for a SISO, minimum-phase, stable NI (resp. SNI) plant $G(s)$ having *relative degree* 0, 1 *or* 2 following the positive feedback IMC scheme shown in Fig. 4. It also facilitates perfect steady-state tracking when $G_m(0) = G(0)$, as discussed in Remark 2.

Lemma 3. *Let $G(s)$ be a SISO, minimum-phase stable NI (resp. SNI) plant having relative degree 0, 1 or 2 and $G_m(s)$ be a stable NI (resp. SNI) model of the plant. Let $N_m(s)$ and $D_m(s)$ be the polynomials such that $G_m(s) = \frac{N_m(s)}{D_m(s)}$. Let $F(s) = \dfrac{k}{s^2 + bs + k}$ be the desired nominal closed-loop transfer function with $k, b > 0$. Then, the controller $C(s) = \dfrac{kD_m(s)}{N_m(s)(s^2 + bs + 2k)}$ is SNI (resp. stable NI) and stabilises the positive feedback IMC scheme shown in Fig. 4 if $G_m(0) \geq G(0) > 0$ and*

$$2k^2\big[D_{mr}(\omega)N_{mi}(\omega) - D_{mi}(\omega)N_{mr}(\omega)\big] + \omega kb\big[D_{mr}(\omega) N_{mr}(\omega) + D_{mi}(\omega)N_{mi}(\omega)\big] + \omega^2 k\big[D_{mi}(\omega)N_{mr}(\omega) - D_{mr}(\omega)N_{mi}(\omega)\big] > 0 \;\; (\text{resp. } \geq 0) \quad \forall \omega \in (0, \infty). \tag{2}$$

Furthermore if $r(\infty)$ is a finite constant, $y(\infty) = \dfrac{\left(\frac{G(0)}{G_m(0)}\right)}{2-\left(\frac{G(0)}{G_m(0)}\right)} r(\infty)$ is also finite. $y(t)$ and $r(t)$ denote respectively the output and reference input signals.

Proof. We begin this proof by recalling the transfer function decomposition $G_m(j\omega) = \frac{N_m(j\omega)}{D_m(j\omega)} = \frac{N_{mr}(\omega)+jN_{mi}(\omega)}{D_{mr}(\omega)+jD_{mi}(\omega)}$. The filter transfer function is considered as $F(s) = \dfrac{k}{s^2 + bs + k}$. Then, the controller transfer function can be expressed as:

$$C(j\omega) = \frac{k(D_{mr}(\omega) + jD_{mi}(\omega))}{(N_{mr}(\omega) + jN_{mi}(\omega))(-\omega^2 + j\omega b + 2k)}. \tag{3}$$

To show that $C(s)$ satisfies the SNI (resp. stable NI) property, we write

$$j\left[C(j\omega) - C(j\omega)^*\right] = \frac{\alpha(\omega)}{\beta(\omega)} \tag{4}$$

where $\alpha(\omega) = 4k^2\big[D_{mr}(\omega)N_{mi}(\omega) - D_{mi}(\omega)N_{mr}(\omega)\big] + 2\omega kb \big[D_{mr}(\omega)N_{mr}(\omega) + D_{mi}(\omega)N_{mi}(\omega)\big] + 2\omega^2 k \big[D_{mi}(\omega) N_{mr}(\omega) - D_{mr}(\omega)N_{mi}(\omega) \big]$ and $\beta(\omega) = \omega^2 b^2 N_{mr}^2(\omega) + \big[\omega^2 N_{mr}(\omega) - 2kN_{mr}(\omega)\big]^2 + \omega^2 b^2 N_{mi}^2(\omega) + \big[\omega^2 N_{mi}(\omega) - 2kN_{mi}(\omega)\big]^2$. Now, $\beta(\omega) > 0 \; \forall \, \omega \in (0, \infty)$ as it has all squared terms with positive signs and $\alpha(\omega)$ is restricted to be positive (resp. non-negative) for all $\omega \in (0, \infty)$ via (2). Hence, $C(s)$ is SNI (resp. stable NI) via design with $C(0) > 0$ as $G_m(0) > 0$. $C(s)$ also stabilises the stable NI (resp. SNI) plant $G(s)$ in a positive feedback loop satisfying the DC loop gain condition $C(0)G(0) \leq C(0)G_m(0) = \frac{kD_m(0)}{2kN_m(0)} \times \frac{N_m(0)}{D_m(0)} = \frac{1}{2} < 1$. It can also be readily shown that $y(\infty) = \dfrac{\left(\frac{G(0)}{G_m(0)}\right)}{2-\left(\frac{G(0)}{G_m(0)}\right)} r(\infty)$ when $r(\infty)$ is a finite constant. This completes the proof. ■

Although Lemma 3 has been derived for SISO systems, it can be readily extended to MIMO systems having a diagonal transfer function matrix.

Remark 1. The frequency-domain design methodology remains effective for SISO and a class of MIMO systems having a decoupled (or diagonal) transfer function matrix. However, this methodology may not be straightforward for general MIMO systems (i.e., other than the decoupled ones) since the procedure involves a lengthy hand-driven calculations. For such systems, the LMI-based design technique is pretty more convenient and useful.

Remark 2. It can be readily shown that a SISO IMC controller $C(s)$ designed via Lemma 3 achieves faithful steady-state tracking even in the case of a model mismatch as long as the DC gains of the plant and its model remain the same [i.e. $G(0) = G_m(0)$]. This is an advantage of the proposed scheme because in practice, it is nearly impossible to identify a perfect model of the plant; however, the steady-state gain $G(0)$ can be measured with a high degree of accuracy. From Fig. 4, the closed-loop transfer function is given by $T(s) = \frac{G(s)C(s)}{1-G(s)C(s)}$ where $C(s) = \frac{Q(s)}{1+G_m(s)Q(s)}$ and $Q(s) = G_m(s)^{-1}F(s)$. Hence, $T(0) = \frac{G(0)G_m(0)^{-1}F(0)}{\left[1+F(0)-G(0)G_m(0)^{-1}F(0)\right]} = F(0)$ and $F(0) = +1$ on noting that $G_m(0) = G(0)$.

Remark 3. The frequency-domain approach offers complete freedom in choosing the filter dynamics $F(s)$ by solving a simple constrained least-square estimation problem (illustrated in Section 4.2.1 via a case study). As the closed-loop response $y(t)$ of the IMC scheme (Fig. 4) is predominantly governed by the filter, the frequency-domain design approach can be conveniently used to meet the desired transient performance criteria. However, this method may not be effective for MIMO systems (other than the decoupled ones) since the procedure involves a lengthy hand-driven calculations.

Remark 4. Since the controller $C(s)$ in Lemma 3 inverts the nominal plant model $G_m(s)$ in its construction, it is sensible to ensure that $G_m(s)$ does not have lightly damped poles and zeros even when the actual plant $G(s)$ has lightly damped poles and zeros.

3.2. An LMI-based design approach

Here, we present the LMI-based synthesis technique.

Theorem 2. *Let $G(s) \in \mathscr{RH}_\infty^{m\times m}$ be a minimum-phase NI plant and $G_m(s) \in \mathscr{RH}_\infty^{m\times m}$ be a minimum-phase NI-model of the plant with $G_m(0) \geq G(0) > 0$. Let $d(s)$ be a stable polynomial such that $H(s) = \frac{1}{d(s)} G_m(s)^{-1}$ is strictly proper. Let $H(s)$ have a minimal state-space realisation $\left[\begin{array}{c|c} A_H & B_H \\ \hline C_H & 0 \end{array}\right]$ with a full-rank C_H matrix. Suppose there exist real matrices $\bar{A}$, $\bar{B}$, $\bar{C}$, $\bar{D}$, $Y = Y^\top$ and $X = X^\top$ of appropriate dimensions such that*

$$\begin{bmatrix} \Phi_{11} & \left(\bar{A}^\top + A_H\right) \\ \left(\bar{A}^\top + A_H\right)^\top & \Phi_{22} \end{bmatrix} < 0, \tag{5a}$$

$$\begin{bmatrix} \Phi_{13} \\ \bar{B} + \bar{A}C_H^\top \end{bmatrix} = 0, \tag{5b}$$

$$\begin{bmatrix} \Phi_{11} & \left(\bar{A}^\top + A_H\right) & YC_H^\top \\ \left(\bar{A}^\top + A_H\right)^\top & \Phi_{22} & C_H^\top \\ C_H Y & C_H & -I_m \end{bmatrix} \leq 0, \tag{5c}$$

$$\begin{bmatrix} Y & I_n \\ I_n & X \end{bmatrix} > 0 \quad \text{and} \tag{5d}$$

$$G_m(0)^{\frac{1}{2}} \left[C_H Y C_H^\top\right] G_m(0)^{\frac{1}{2}} < I_m, \tag{5e}$$

with the following shorthand

$$\begin{cases} \Phi_{11} = A_H Y + Y A_H^\top + B_H \bar{C} + \bar{C}^\top B_H^\top, \\ \Phi_{13} = B_H \bar{D} + A_H Y C_H^\top + B_H \bar{C} C_H^\top, \\ \Phi_{22} = X A_H + A_H^\top X. \end{cases} \tag{6}$$

Construct an auxiliary system $\Sigma(s)$ *as* $\Sigma(s) = D_\Sigma + C_\Sigma \big(sI - A_\Sigma\big)^{-1} B_\Sigma$ *where*

$$\begin{cases} D_\Sigma = \bar{D}, \\ C_\Sigma = \bar{C} N^{-\top}, \\ B_\Sigma = M^{-1}(\bar{B} - X B_H \bar{D}), \\ A_\Sigma = M^{-1}\big(\bar{A} - X A_H Y - X B_H \bar{C}\big) N^{-\top}, \end{cases} \tag{7}$$

and M *and* N *are square and non-singular solutions of the algebraic equation* $NM^\top = I_n - YX$*. Then, the controller* $C(s) = H(s)\Sigma(s)$ *is SSNI and asymptotically stabilises the positive feedback IMC scheme shown in Fig. 4.*

Proof. We begin the proof on noting that $C(s) = Q(s)\big[I + G_m(s)Q(s)\big]^{-1}$ where the Youla parameter matrix $Q(s)$ is parametrised as $Q(s) = G_m(s)^{-1}F(s)$. $F(s)$ plays the role of a low-pass filter, which is to be determined. We first choose a stable polynomial $d(s)$ such that $\frac{1}{d(s)}G_m(s)^{-1}$ is strictly proper. Accordingly, $Q(s) = G_m(s)^{-1}F(s)$ is modified to $Q(s) = \frac{1}{d(s)}G_m(s)^{-1}\bar{F}(s)$ where $\bar{F}(s) = d(s)F(s)$ is assumed proper through an appropriate choice of $F(s)$. Now, $\bar{F}(s)$ is to be determined instead of $F(s)$. Denote $H(s) = \frac{1}{d(s)}G_m(s)^{-1}$ and let $H(s)$ have a minimal state-space $\left[\begin{array}{c|c} A_H & B_H \\ \hline C_H & 0 \end{array}\right]$. We then obtain the expression of the controller $C(s) = Q(s)\big[I + G_m(s)Q(s)\big]^{-1} = H(s)\left(\bar{F}(s)\big[I + F(s)\big]^{-1}\right)$ substituting $Q(s) = H(s)\bar{F}(s)$. Denote $\Sigma(s) = \bar{F}(s)\big[I + F(s)\big]^{-1}$ and let $\Sigma(s)$ have a minimal state-space realisation $\left[\begin{array}{c|c} A_\Sigma & B_\Sigma \\ \hline C_\Sigma & D_\Sigma \end{array}\right]$. We then derive the state-space representation of the controller $C(s) = H(s)\Sigma(s)$ as $\left[\begin{array}{c|c} A_c & B_c \\ \hline C_c & D_c \end{array}\right] = \left[\begin{array}{cc|c} A_H & B_H C_\Sigma & B_H D_\Sigma \\ 0 & A_\Sigma & B_\Sigma \\ \hline C_H & 0 & 0 \end{array}\right]$. We are now ready to derive the proof of this theorem, which has been divided into two main parts for easy understanding.

Part I: To show that $C(s)$ ***is SSNI***

The designed controller $C(s) = \left[\begin{array}{c|c} A_c & B_c \\ \hline C_c & D_c \end{array}\right]$ is SSNI if there exists a real matrix $\mathscr{Y} = \mathscr{Y}^\top > 0$ of appropriate dimension such that

$$\begin{cases} A_c\mathscr{Y} + \mathscr{Y}A_c^\top < 0, \qquad \text{and} \\ B_c + A_c\mathscr{Y}C_c^\top = 0, \end{cases} \tag{8}$$

via Lemma 2 and the pair (A_c, C_c) remains observable. However, the conditions in (8) are not in an LMI form as the terms $A_c\mathscr{Y}$ and $A_c\mathscr{Y}C_c^\top$ contain products of the unknown matrix variables. Therefore, a linearising change in the controller variables is required to transform (8) into an LMI form.

Linearisation process (i.e. conversion to LMI form): As a first step towards the linearisation process, we partition $\mathscr{Y}$ and $\mathscr{Y}^{-1}$ below following the technique proposed in (Scherer et al., 1997).

$$\mathscr{Y} = \begin{pmatrix} Y & N \\ N^\top & \bullet \end{pmatrix} \quad \text{and} \quad \mathscr{Y}^{-1} = \begin{pmatrix} X & M \\ M^\top & \bullet \end{pmatrix} \tag{9}$$

where $Y = Y^\top \in \mathbb{R}^{n\times n}$, $X = X^\top \in \mathbb{R}^{n\times n}$ and the symbol $\bullet$ represents the matrices that are not explicitly used in the linearisation process. Note $\mathscr{Y}^{-1}$ exists since $\mathscr{Y} > 0$. Note also that X, Y, M, N are not independent LMI variables but must satisfy $NM^\top = I_n - YX$ (Scherer et al., 1997). Since M and N are square and non-singular (Scherer et al., 1997), the following block matrices

$$\Pi_1 = \begin{pmatrix} I_n & X \\ 0 & M^\top \end{pmatrix} \quad \text{and} \quad \Pi_2 = \begin{pmatrix} Y & I_n \\ N^\top & 0 \end{pmatrix} \tag{10}$$

are also non-singular. Π_1 and Π_2 are related through the expression $\mathscr{Y}\Pi_1 = \Pi_2$, which has been obtained from the fundamental relationship $\mathscr{Y}\mathscr{Y}^{-1} = I$ (Scherer et al., 1997). The positive definiteness of the Lyapunov candidate matrix $\mathscr{Y} = \begin{pmatrix} Y & N \\ N^\top & \bullet \end{pmatrix}$ is guaranteed by (5d) via the congruence transformation shown below:

$$\Pi_1^\top \mathscr{Y} \Pi_1 = \begin{pmatrix} Y & I_n \\ I_n & X \end{pmatrix} > 0. \tag{11}$$

Applying another congruence transformation on (8) with the help of $\operatorname{diag}\{\Pi_1, I\}$, we obtain

$$\begin{cases} \Pi_1^\top \left(A_c\mathscr{Y} + \mathscr{Y}A_c^\top\right)\Pi_1 < 0, \qquad \text{and} \\ \Pi_1^\top \left(B_c + A_c\mathscr{Y}C_c^\top\right) = 0. \end{cases} \tag{12}$$

Then, inserting a new set of matrix variables

$$\begin{cases} \bar{A} = M A_\Sigma N^\top + X A_H Y + X B_H C_\Sigma N^\top, \\ \bar{B} = M B_\Sigma + X B_H D_\Sigma, \\ \bar{C} = C_\Sigma N^\top, \quad \text{and} \\ \bar{D} = D_\Sigma, \end{cases} \tag{13}$$

into (12), we obtain

$$\begin{cases} \begin{bmatrix} \Phi_{11} & \left(\bar{A}^\top + A_H\right) \\ \left(\bar{A}^\top + A_H\right)^\top & \Phi_{22} \end{bmatrix} < 0, \qquad \text{and} \\ \begin{bmatrix} \Phi_{13} \\ \bar{B} + \bar{A}C_H^\top \end{bmatrix} = 0. \end{cases} \tag{14}$$

These two conditions are linear in $\bar{A}$, $\bar{B}$, $\bar{C}$, $\bar{D}$, $Y > 0$, $X > 0$ and they are indeed the same as (5a) and (5b). At this stage, we are only left to show that the pair (A_c, C_c) is observable.

Observability of $(\mathbf{A_c}, \mathbf{C_c})$: The pair (A_c, C_c) is observable via (5c) since the associated Observability Gramian (Boyd, El Ghaoui, Feron, & Balakrishnan, 1994) condition $\mathscr{P}A_c + A_c^\top\mathscr{P} + C_c^\top C_c \le 0 \Leftrightarrow A_c\mathscr{Y} + \mathscr{Y}A_c^\top + \mathscr{Y}C_c^\top C_c\mathscr{Y} \le 0$, where $\mathscr{Y} = \mathscr{P}^{-1} > 0$, is equivalent to (5c) via a congruence transformation with respect to $\operatorname{diag}\{\Pi_1, I_m\}$ and taking a Schur complement (Boyd et al., 1994). Note also that the matrix $C_c = \begin{bmatrix} C_H & 0 \end{bmatrix}$ has full row-rank since $\operatorname{rank}[C_H] = m$ via assumption. This implies from the expression $B_c + A_c\mathscr{Y}C_c^\top = 0$ that B_c has full column-rank since $\mathscr{Y} > 0$ and A_c is Hurwitz via (5a).

Hence, the LMI conditions (5a)–(5d) jointly ensure that $C(s)$ is SSNI via Lemma 2.

Reconstruction of $\mathbf{\Sigma(s)}$, $\mathbf{F(s)}$ and $\mathbf{C(s)}$: Reconstruct the auxiliary filter $\Sigma(s) = D_\Sigma + C_\Sigma\big(sI - A_\Sigma\big)^{-1}B_\Sigma$ via

$$\begin{cases} D_\Sigma = \bar{D}, \\ C_\Sigma = \bar{C} N^{-\top}, \\ B_\Sigma = M^{-1}(\bar{B} - X B_H \bar{D}), \\ A_\Sigma = M^{-1}\big(\bar{A} - X A_H Y - X B_H \bar{C}\big) N^{-\top}, \end{cases}$$

where M and N are square and non-singular solutions[1] of the algebraic equation $NM^\top = I_n - YX$. From the knowledge of

[1] Note that the solutions M and N are not unique. A convenient choice can be suggested as $M = I_n$ and $N = I_n - YX$ or $N = I_n$ and $M = I_n - XY$.

$\Sigma(s)$, retrieve the filter $F(s)$ relying on the relationship $F(s) = \frac{1}{d(s)}\Sigma(s)\left[I - \frac{1}{d(s)}\Sigma(s)\right]^{-1}$. Finally, we also construct the Youla parameter $Q(s) = G_m(s)^{-1}F(s)$ and the desired controller $C(s) = Q(s)\big[I + G_m(s)Q(s)\big]^{-1} = H(s)\Sigma(s) = \frac{1}{d(s)}G_m(s)^{-1}\Sigma(s)$.

Part II: DC loop gain condition holds

The inequality condition (5e) is equivalent to $G_m(0)^{\frac{1}{2}}\ C(0)\ G_m(0)^{\frac{1}{2}} < I_m$ since $C(0) = C_c\mathscr{Y}C_c^\top = C_H Y C_H^\top$. This, in turn, is equivalent to $\lambda_{\max}[C(0)G_m(0)] < 1$ via Lanzon and Petersen (2008). As $G_m(0) \geq G(0) > 0$ via assumption and $C(0) > 0$ via construction, the preceding condition implies $\lambda_{\max}[C(0)G(0)] < 1$.

Therefore, Part I and Part II together prove that the positive feedback interconnection (in Fig. 4) of $C(s)$, being SSNI, and $G(s)$, being a stable and minimum-phase NI system, satisfies all the assumptions of Theorem 1, as well as the DC loop gain condition. Hence, the interconnection is asymptotically stable. ■

Remark 5. Unlike the frequency-domain approach, the LMI-based IMC design approach can conveniently and efficiently handle higher-order and MIMO systems. However, in the LMI approach, the filter function $F(s)$ is not explicitly selected by the designer. It is reconstructed from the variables obtained from the LMI solutions. Therefore, we cannot guarantee the fulfilment of all desired closed-loop performance criteria "a priori" via this approach. In this situation, the choice of the polynomial $d(s)$ becomes crucial as $d(s)$ is the only design parameter that can be selected "a priori" to achieve a desired closed-loop response.

Remark 6. A necessary and sufficient condition for the stability of an IMC scheme where $G(s)$ is open-loop stable is that the Youla parameter $Q(s)$ must be stable. In the proposed NI-based IMC scheme shown in Fig. 4, $Q(s) = C(s)\,[I - G_m(s)C(s)]^{-1}$, which can be treated as a positive feedback interconnection between $C(s)$ and $G_m(s)$. $Q(s)$ can be readily shown to be stable. Since $G_m(s)$ is stable NI and $C(s)$ is designed to be SNI/SSNI (either via the frequency-domain approach or via the LMI-based methodology) satisfying the condition $\lambda_{\max}[C(0)G_m(0)] < 1$, Theorem 2 guarantees the closed-loop stability of the positive feedback IMC scheme (in Fig. 4), which, in turn, implies the stability of $Q(s)$.

3.3. Steady-state tracking performance of the LMI-based (NI) IMC scheme

The following lemma shows that under a reasonable and practically feasible assumption $G_m(0) = G(0) > 0$, a perfect steady-state tracking can be achieved by the proposed scheme if the inequality condition (5e) is replaced by the equality condition $G_m(0)^{\frac{1}{2}}C_H Y C_H^\top G_m(0)^{\frac{1}{2}} = \frac{1}{2}I_m$, keeping (5a)–(5d) intact.

Lemma 4. *Let $G(s) \in \mathscr{RH}_\infty^{m\times m}$ be a minimum-phase NI plant with a known $G(0)$. Suppose $G_m(0) = G(0) > 0$. Then, the NI-based IMC scheme, developed in Theorem 2, achieves a perfect steady-state tracking (i.e. $\lim_{t\to\infty}\big[-r(t) + y(t)\big] = 0$) where $\lim_{t\to\infty} r(t) = r_{ss}$ is a finite constant if the condition (5e) in Theorem 2 is modified to $G_m(0)^{\frac{1}{2}}\left[C_H Y C_H^\top\right]G_m(0)^{\frac{1}{2}} = \frac{1}{2}I_m$.*

Proof. The closed-loop transfer function matrix from the reference input r to the output y of the IMC scheme, shown in Fig. 4, is given by $T(s) = G(s)C(s)\big[I - G(s)C(s)\big]^{-1}$. Now, substituting the expression $C(s) = G_m(s)^{-1}F(s)\big[I + F(s)\big]^{-1}$ and upon simplifying, we get $T(s) = G(s)G_m(s)^{-1}F(s)\big[I + F(s) - G(s)G_m(s)^{-1}F(s)\big]^{-1}$. This readily implies $T(0) = F(0)$ when $G_m(0) = G(0)$. Furthermore, $G_m(0)^{\frac{1}{2}}\left[C_H Y C_H^\top\right]G_m(0)^{\frac{1}{2}} = \frac{1}{2}I_m \Leftrightarrow G_m(0)^{\frac{1}{2}}C(0)\ G_m(0)^{\frac{1}{2}} = \frac{1}{2}I_m \Leftrightarrow G_m(0)^{-1}F(0)\big[I + F(0)\big]^{-1} = \frac{1}{2}G_m(0)^{-1} \Rightarrow F(0) = I$. This hence ensures that $y_{ss} = \lim_{t\to\infty} y(t) = \lim_{s\to 0} sY(s) = \lim_{s\to 0} sT(s)R(s) = \lim_{s\to 0} sF(s)\,R(s) = F(0)\lim_{s\to 0} sR(s) = r_{ss}$, since $F(0) = I$ and on noting that $\lim_{s\to 0} sR(s) = r_{ss}$ is constant. ■

Remark 7. Lemma 4 proves that the NI-based IMC scheme proposed via Theorem 2 facilitates perfect steady-state reference tracking, when $r(\infty)$ exists, despite a model mismatch [i.e. when $G_m(s) \neq G(s)$] as long as $G_m(0) = G(0)$. This is not an overly restrictive assumption because, in practice, it is possible to measure the steady-state gain (i.e. the DC-gain) of a plant accurately. In that case, it is also possible to identify a reasonably accurate plant model $G_m(s)$ having the same DC-gain as that of the real plant. However, the robust stability of the IMC scheme (in Fig. 4) remains unaffected in the presence of a model mismatch as long as $G(0) \leq G_m(0)$ since the closed-loop stability depends only the DC loop gain condition $\lambda_{\max}[C(0)G(0)] < 1$, as established in Theorem 2.

3.4. Guidelines on how to choose the polynomial $d(s)$

The choice of the stable polynomial $d(s)$ that we will now suggest is based on empirical analysis rather than a theoretical analysis. We have considered four different models $G_{m_1}(s)$, $G_{m_2}(s)$, $G_{m_3}(s)$ and $G_{m_4}(s)$ of a cantilever beam conforming with the practical setup shown in Fig. 2. The first model is a second-order system $G_{m_1}(s) = \frac{1}{s^2+0.2s+1}$, which has its resonant mode at $\omega = 1$ rad/s. The next model is still a second-order system $G_{m_2}(s) = \frac{13}{s^2+0.1s+358}$, but it has a higher resonant frequency of $\omega = 19$ rad/s. After that, we consider a fourth-order model $G_{m_3}(s) = \frac{1}{s^2+0.2s+2} + \frac{4}{s^2+0.23s+9}$ having two resonant modes at $\omega = 1.41$ rad/s and $\omega = 3$ rad/s respectively. Finally, we take a sixth-order model $G_{m_4}(s) = \frac{1}{s^2+0.2s+2} + \frac{4}{s^2+0.23s+9} + \frac{7}{s^2+0.15s+13}$ having three resonant modes at $\omega = \{1.37,\ \ 2.93,\ \ 3.6\}$ rad/s respectively.

For each of the four plant models, we have taken thirty different $d(s)$ candidates as mentioned in Tables 1–4 [Appendix] and accordingly, found thirty controller transfer functions $\{C_1(s), C_2(s), \ldots, C_{30}(s)\}$ using the LMI-based design algorithm. Fig. 5(a) shows the Bode plots of the set of thirty closed-loop transfer functions $T_i(s) = \frac{G_{m_1}(s)C_i(s)}{1-G_{m_1}(s)C_i(s)}$ $\forall i \in \{1, 2, \ldots, 30\}$ corresponding to $\{d_1(s),\ d_2(s),\ \ldots, d_{30}(s)\}$ chosen for $G_{m_1}(s)$. Similarly, Figs. 6(a), 7(a) and 8(a) show the Bode plots of the three sets of closed-loop transfer functions $T_j(s) = \frac{G_{m_2}(s)C_j(s)}{1-G_{m_2}(s)C_j(s)}$ $\forall j \in \{1, 2, \ldots, 30\}$; $T_k(s) = \frac{G_{m_3}(s)C_k(s)}{1-G_{m_3}(s)C_k(s)}$ $\forall k \in \{1, 2, \ldots, 30\}$; and $T_l(s) = \frac{G_{m_4}(s)C_l(s)}{1-G_{m_4}(s)C_l(s)}$ $\forall l \in \{1, 2, \ldots, 30\}$. Whereas, Figs. 5(b), 6(b), 7(b) and 8(b) show the impulse responses of each of the above four sets (each set consists of thirty transfer functions) of the closed-loop systems $T_i(s)$, $T_j(s)$, $T_k(s)$ and $T_l(s)$. The choice of each set of polynomials $\{d_1(s), d_2(s), \ldots, d_{30}(s)\}$ depends primarily on the resonant modes of the plant model. They are constructed such that some of the roots are real and slower, some of them are real and faster, and the remaining are complex. This wide range of test cases and their comparative study with respect to the time-domain performance criteria (e.g. peak overshoot, settling/decaying time, damping, etc.) help us to suggest useful guidelines for selecting an appropriate $d(s)$ for a given plant model.

Below, we summarise our findings on the effect of $d(s)$ on the closed-loop response of the NI-based IMC scheme:

- **Bandwidth:** A leftward-shift of the negative real roots of $d(s)$ or an increase in the natural frequency of complex roots increases the bandwidth of the closed-loop system;

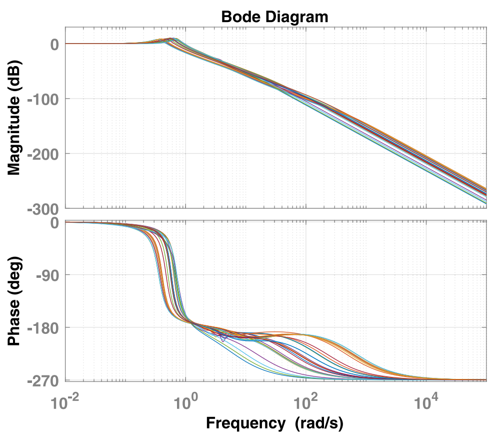

(a)

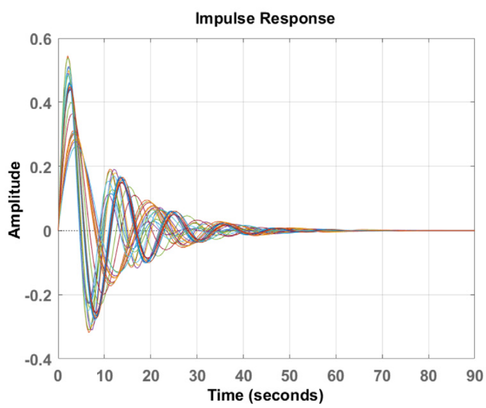

(b)

Fig. 5. (a) Bode plots of the closed-loop transfer functions $T_i(s) = \frac{G_{m_1}(s)C_i(s)}{1-G_{m_1}(s)C_i(s)}$ $\forall i \in \{1, 2, \dots, 30\}$ corresponding to $\{d_1(s), d_2(s), \dots, d_{30}(s)\}$ as mentioned in Table 1; (b) Impulse responses of $T_i(s)$ for all i.

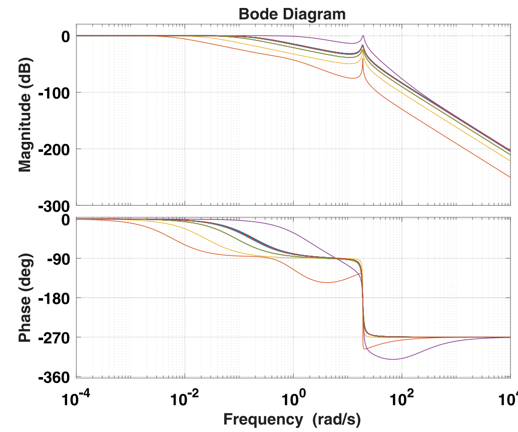

(a)

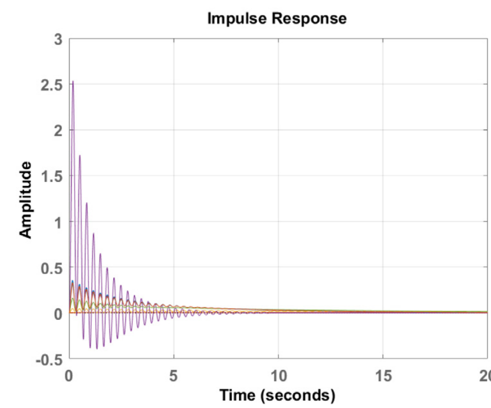

(b)

Fig. 6. (a) Bode plots of the closed-loop transfer functions $T_j(s) = \frac{G_{m_2}(s)C_j(s)}{1-G_{m_2}(s)C_j(s)}$ $\forall j \in \{1, 2, \dots, 30\}$ corresponding to $\{d_1(s), d_2(s), \dots, d_{30}(s)\}$ as mentioned in Table 2; (b) Impulse responses of $T_j(s)$ for all j.

- **Settling time:** A leftward-shift of the roots of $d(s)$ decreases the settling time of the step (resp. impulse) response. However, a substantial left-shift may also increase the settling time as the closed-loop system becomes more oscillatory. On the other hand, changing the imaginary parts of the complex roots of $d(s)$ whilst keeping the real parts unchanged does not have any significant impact on the settling time;
- **Peak overshoot:** A leftward-shift of the negative real roots of $d(s)$ or an increase in the natural frequency of complex roots increases the speed of the step and impulse responses, but at the cost of an higher peak overshoot;
- **Fastest controller pole:** A leftward-shift of the real or complex roots of $d(s)$ drives the controller poles to be faster. However, this causes an increase in the control input demand.

Let 'r' be the relative degree of $G_m(s)$ [i.e. $\lim_{s\to\infty} s^i G_m(s) = 0 \ \forall i \in \{0, 1, 2, \dots, r-1\}$ and $\lim_{s\to\infty} s^r G_m(s) \neq 0$]. $\mathbb{D}\big[G_m(s)\big]$ denotes the polynomial whose roots are the fastest 'r' poles of $G_m(s)$. For example, if $G_m(s) = \begin{bmatrix} \frac{s+z_1}{(s+p_1)(s^2+a_1s+a_0)} & \frac{k_1}{(s^2+a_1s+a_0)} \\ \frac{k_2}{(s^2+a_1s+a_0)} & \frac{s+z_2}{(s+p_2)(s^2+a_1s+a_0)} \end{bmatrix}$, then $\mathbb{D}\big[G_m(s)\big] = (s+p_1)(s+p_2)(s^2+a_1s+a_0)$. From the extensive simulation studies shown in Figs. 5(a)–8(a) and Figs. 5(b)–8(b) and Tables 1–4, we observe that a choice of $d(s) = (s+a)\mathbb{D}\big[G_m(s)\big]$, where the parameter a is selected as the frequency of the first resonant mode of $G_m(s)$, offers an acceptable trade-off between the speed of response and the settling time. It does not also result in too-fast controller poles, which inevitably demand higher control effort. However, this choice may increase the peak overshoot of the impulse response. In applications where a reduction in the peak overshoot is preferable over the other time-domain performance criteria, one could choose the real root $s = -a$ of $d(s)$ at one or two decade(s) below the frequency of the first resonant mode of $G_m(s)$.

Remark 8. In the LMI-based IMC design approach, the formulation $H(s) = \frac{1}{d(s)} G_m(s)^{-1}$ introduces the inverse dynamics of the model $G_m(s)$ into the controller $C(s) = H(s)\Sigma(s)$. If the $G_m(s)$ has poorly damped zeros or highly resonant interlacing pole-zero pairs, we can choose $d(s) = (s+a)^p$ instead of the earlier choice $d(s) = (s+a)\mathbb{D}\big[G_m(s)\big]$. The parameter a is selected as the frequency of the first resonant mode of $G_m(s)$ as before and $p \geq r+1$ such that $\frac{1}{d(s)} G_m(s)^{-1}$ remains strictly proper (preferably with relative degree equal to one). This choice of $d(s)$ results in a reduced peak overshoot of the closed-loop step/impulse response, but at the cost of compromising the speed.

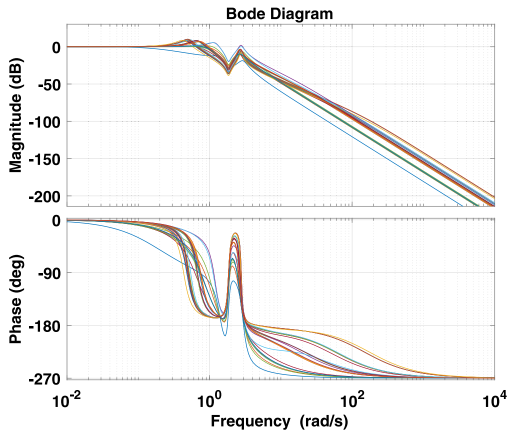

(a)

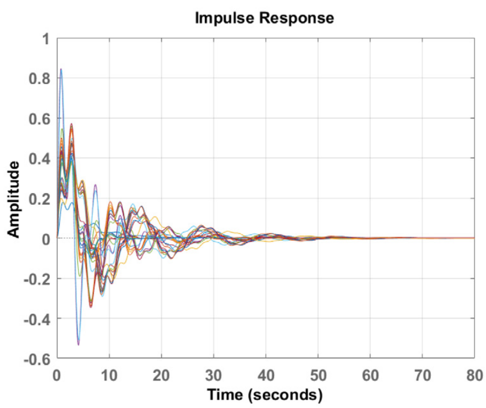

(b)

Fig. 7. (a) Bode plots of the closed-loop transfer functions $T_k(s) = \frac{G_{m_3}(s)C_k(s)}{1-G_{m_3}(s)C_k(s)}$ $\forall k \in \{1, 2, \ldots, 30\}$ corresponding to $\{d_1(s), d_2(s), \ldots, d_{30}(s)\}$ as mentioned in Table 3; (b) Impulse responses of $T_k(s)$ for all k.

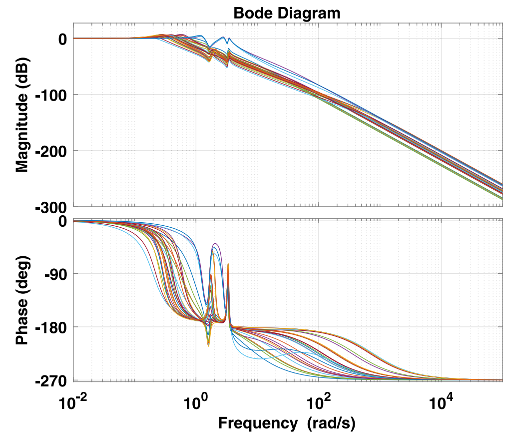

(a)

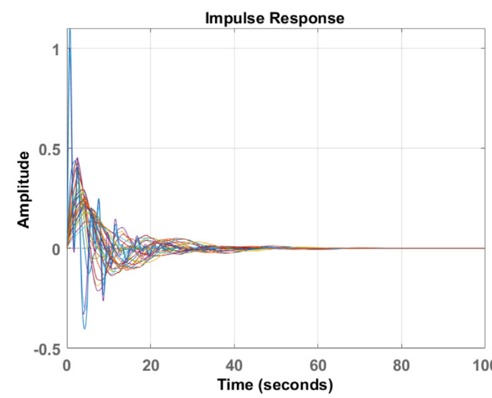

(b)

Fig. 8. (a) Bode plots of the closed-loop transfer functions $T_l(s) = \frac{G_{m_4}(s)C_l(s)}{1-G_{m_4}(s)C_l(s)}$ $\forall l \in \{1, 2, \ldots, 30\}$ corresponding to $\{d_1(s), d_2(s), \ldots, d_{30}(s)\}$ as mentioned in Table 4; (b) Impulse responses of $T_l(s)$ for all l.

4. Case study on a vibration suppressor: Simulation results with experimental validation

This section will apply the proposed NI-based IMC scheme for the vibration control of a lightweight cantilever beam attached to a fixed end. The custom-made vibration suppressor system shown in Fig. 9(a) consists of a lightweight aluminium beam clamped at one end and mounted on a solid plate. The plate sits on top of a moving rail powered by a 12 V, 251 rpm metal-geared DC motor. The beam is equipped with a pair of collocated Macro Fibre Composite (MFC) sensor and actuator patches.

4.1. System identification of the vibration suppressor

For the system identification purpose, we used the Matlab System Identification Toolbox to transform the time-series data (experimentally generated or obtained) into frequency-domain and obtained a fourth-order model of the system given by

$$G_m(s) = \frac{30050\,(s^2 + 1.996s + 7631)}{(s^2 + 1.108s + 6350)(s^2 + 28.43s + 2.21 \times 10^5)}.$$

$G_m(s)$ is indeed a stable and minimum-phase transfer function having relative degree 2. Fig. 9(b) reveals that the identified model $G_m(s)$ is truly a good replica of the physical plant (i.e. the vibration suppressor shown in Fig. 2), especially at the low-frequency range. Moreover, the identified model $G_m(s)$ is stable NI, as confirmed by the red-coloured Bode plot in Fig. 9(b).

4.2. NI-based internal model controller (IMC) design

This subsection will design the NI-based IMC controllers for the vibration suppressor system following the frequency-domain and LMI-based design methodologies introduced in Sections 3.1 and 3.2. After that, we will examine the feasibility, effectiveness and performance of the designed controllers via simulation case studies and hardware experiments. A performance comparison between the two methodologies is also provided.

4.2.1. Frequency-domain approach

We first decompose the plant model as $G_m(j\omega) = \frac{N_m(j\omega)}{D_m(j\omega)} = \frac{N_{mr}(\omega) + jN_{mi}(\omega)}{D_{mr}(\omega) + jD_{mi}(\omega)}$ where $D_{mr}(\omega) = \omega^4 - 2.272 \times 10^5\omega^2 + 1.41 \times 10^9$, $D_{mi}(\omega) = 4.017 \times 10^5\omega - 29.75\omega^3$, $N_{mr}(\omega) = 2.293 \times 10^8 - 30050\omega^2$ and $N_{mi}(\omega) = 5.998 \times 10^4$. Since $G_m(s)$ has relative degree 2, we choose the filter function $F_1(s) = \frac{k}{(s^2 + bs + k)}$ and the controller $C_1(s) = \frac{kD_m(s)}{N_m(s)(s^2 + bs + 2k)}$ following Lemma 3. The controller parameters $b,\ k > 0$ need to be selected such that $C_1(s)$ becomes SNI (resp. stable NI). Via Lemma 3, $C_1(s)$ is SNI

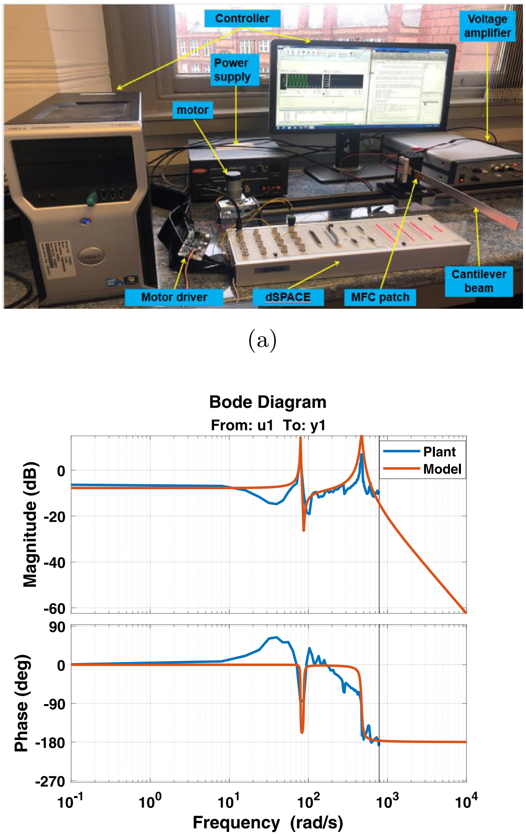

(a)

(b)

Fig. 9. (a) Closed-loop control set-up of the vibration suppressor using the dSPACE platform; and (b) Bode plots of the physical plant $G(s)$ and its identified model $G_m(s)$.

(resp. stable NI) if

$$2k^2(-8.34\times10^5\omega^5+5.27\times10^9\omega^3-7.5\times10^{12}\omega)+$$
$$\omega kb(-30050\,\omega^6+7.06\times10^9\omega^4-9.45\times10^{13}\omega^2+$$
$$3.23\times10^{17})+\omega^2k(8.34\times10^5\omega^5-5.27\times10^9\omega^3+$$
$$7.5\times10^{12}\omega)>0\ \ (\text{resp. }\geq 0)\quad \forall\omega\in(0,\infty).$$

The polynomial in the left-hand side of the above inequality can be rearranged in a convenient form as

$$(8.34\times10^5k-30050kb)\,\omega^7+$$
$$(7.06\times10^9kb-1.67\times10^6k^2-5.27\times10^9k)\,\omega^5+$$
$$(1.05\times10^{10}k^2-9.45\times10^{13}kb-7.5\times10^{12}k)\,\omega^3+$$
$$(3.23\times10^{17}kb-1.50\times10^{13}k^2)\,\omega,$$

which remains positive $\forall\omega\in(0,\infty)$ if the coefficients of all the ω terms take on positive values. This can be mathematically formulated as

$$\begin{bmatrix} 0 & 30050 \\ 1.67\times10^6 & -7.06\times10^9 \\ -1.05\times10^{10} & 9.45\times10^{13} \\ 1.51\times10^{13} & -3.23\times10^{17}\end{bmatrix}\begin{bmatrix}k\\ b\end{bmatrix}\leq\begin{bmatrix}8.34\times10^5\\ -5.27\times10^9\\ -7.5\times10^{12}\\ 0\end{bmatrix}.$$

This can be treated as a constrained, linear, least-square estimation problem, which can readily be solved using the Matlab-based SDP solver packages. We set the lower bounds for k and b as 100 and 20, respectively, so that the filter poles can be placed at $s_{1,2}=-10$. This is entirely an arbitrary choice to ensure that the closed-loop system is neither too sluggish nor too fast. Solving the above least-square estimation problem in CVX (Grant & Boyd, 2014), we get feasible upper bounds of k and b as $k\leq 4.2891\times10^5$ and $b\leq 20$. The filter is then constructed as $F_1(s)=\dfrac{100}{s^2+20s+100}$ and the desired SNI controller is obtained as

$$C_1(s)=\alpha_1(s)/\beta_1(s), \tag{15}$$

where $\alpha_1(s)=3.3278\times10^{-3}(s^2+1.108s+6350)(s^2+28.43s+2.21\times10^5)$ and $\beta_1(s)=(s^2+20s+200)(s^2+1.996s+7631)$. We then verify the DC loop gain condition $C_1(0)G_m(0)=3.0599\times0.1634=0.4999<1$. Hence, the NI-based IMC scheme shown in Fig. 4 is guaranteed to be asymptotically stable via Theorem 1.

4.2.2. LMI-based approach

To proceed with the IMC design following Theorem 2, we choose the polynomial $d(s)=(s+80)\mathbb{D}\big[G_m(s)\big]=(s+80)(s^2+28.43s+2.21\times10^5)$ since the plant model $G_m(s)$ has the first resonant peak at approximately $\omega=80$ rad/s. This choice of $d(s)$ is based on the guidelines presented in Section 3.4 as it offers an acceptable trade-off between speed of response and settling time. Also, choosing $d(s)$ in such a manner helps to avoid fast poles in the controller dynamics. Upon solving the set of LMI conditions (5a)–(5e), we obtain the desired SSNI controller

$$C_2(s)=\frac{14.383(s+1429)}{(s+80)(s+83.97)}. \tag{16}$$

It can be readily verified that the DC loop gain is less than one $[C_2(0)G(0)=C_2(0)G_m(0)=3.0599\times0.1634=0.5000<1]$, which guarantees the closed-loop stability of the IMC scheme shown in Fig. 4.

4.3. Matlab simulation results

This subsection provides a comprehensive Matlab simulation study on the performance of the designed controllers $C_1(s)$ and $C_2(s)$ under an ideal situation [i.e. when $G(s)=G_m(s)$] and a perturbed condition [i.e. when $G(s)\neq G_m(s)$]. The primary control objective of this case study is to reduce the vibration induced in the cantilever beam externally.

4.3.1. Under ideal situation [i.e. when $G(s)=G_m(s)$]

This subsection shows and analyses the regulatory (via *pulse* response) and tracking (via *step* response) performances of the NI-based IMC scheme achieved by the controllers $C_1(s)$ and $C_2(s)$. The open-loop pulse and step responses are respectively shown in Figs. 10(a) and 10(b). Fig. 10(d) shows that in the ideal case, both $C_1(s)$ and $C_2(s)$ achieve a perfect steady-state tracking. In addition, $C_1(s)$ results in a well-damped closed-loop response with no overshoot, while the closed-loop response with $C_2(s)$ exhibits little oscillations. However, the latter offers a remarkable improvement in the settling time (0.29 s) over the former (0.58 s). To analyse the disturbance rejection capacity (subject to a pulse disturbance input), Fig. 10(c) shows that $C_2(s)$ observes a decay time of 0.62 s and a peak overshoot of 0.3537 cm. In contrast, $C_1(s)$ causes a peak overshoot of 0.2789 cm and a settling time of 2.56 s. Note that the peak overshoot [resulted by $C_2(s)$] can be further reduced by choosing a more appropriate $d(s)$, as outlined in Section 3.4, but at the cost of increased settling time. Hence, we can conclude that the performance achieved by the frequency-domain design technique is not that appealing compared to the LMI-based design methodology.

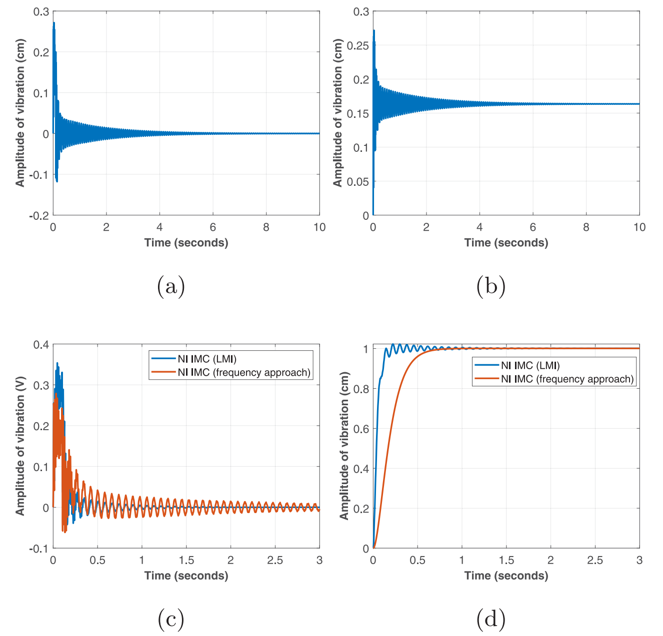

Fig. 10. [When $G(s) = G_m(s)$] (a) Open-loop response to a pulse input; (b) Open-loop response to a unit step input; (c) Closed-loop pulse responses achieved by the controllers $C_1(s)$ [via frequency-domain approach] and $C_2(s)$ [via LMI-based approach]; (d) Closed-loop unit step responses achieved by $C_1(s)$ and $C_2(s)$.

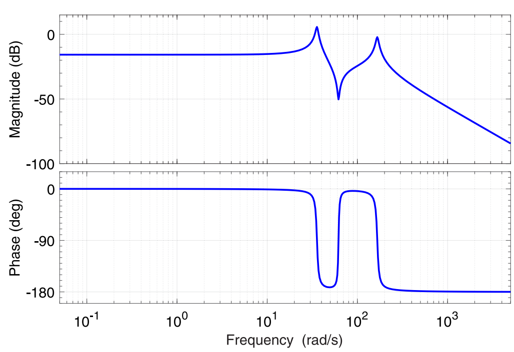

Fig. 11. Bode plot of the cantilever beam $G_\delta(s)$ that is different from $G_m(s)$.

4.3.2. Under perturbed condition [when $G(s) \neq G_m(s)$]

Now, we consider the case where the identified model is not identical to the physical plant [i.e. $G(s) \neq G_m(s)$]. To handle such situations, we impose a reasonable and practically feasible assumption $G(0) = G_m(0)$. Our objective is to test the robustness of the designed controllers $C_1(s)$ and $C_2(s)$ against the model mismatch [i.e. $G(s) \neq G_m(s)$]. To induce a difference between $G(s)$ and $G_m(s)$, we choose a slightly perturbed transfer function of the cantilever beam, denoted as $G_\delta(s)$, given below:

$$G_\delta(s) = \frac{1502.5(s^2 + 1.996s + 3816)}{(s^2 + 2.108s + 1270)(s^2 + 10.43s + 2.763 \times 10^4)}. \quad (17)$$

It can be readily verified that this $G_\delta(s)$ is still a minimum-phase SNI transfer function. Its Bode plot (shown in Fig. 11) also confirms its SNI property. The closed-loop stability of the positive feedback IMC scheme remains preserved for both $C_1(s)$ and $C_2(s)$ since the DC loop gain condition holds in both the cases: $C_1(0)G_\delta(0) = 3.0599 \times 0.1634 = 0.5000 < 1$ and $C_2(0)G_\delta(0) = 3.0599 \times 0.1634 = 0.5000 < 1$.

Figs. 12(a)–12(d) show the open-loop and closed-loop responses of the perturbed plant $G_\delta(s)$ subject to the same pulse and unit step inputs applied in Figs. 10(a)–10(d). The time responses in Figs. 12(c) and 12(d) show that the achieved transient performance has slighted deteriorated compared to Figs. 10(c) and 10(d) due to the induced model mismatch. Fig. 12(c) reveals that although the reduction in the peak value in the closed-loop response is negligible, the decay of oscillation is significant. Besides, it also reveals that $C_2(s)$ performs better than $C_1(s)$. Fig. 12(d) indicates that both $C_1(s)$ and $C_2(s)$ achieve perfect steady-state tracking although $C_2(s)$ offers a faster dynamic performance than $C_1(s)$. Note that both $C_1(s)$ and $C_2(s)$ have been able to achieve perfect nominal steady-state tracking despite the model mismatch (as reflected in Fig. 12(d)) only due to the fact that $G_m(0) = G_\delta(0)$. If $G_m(0) \neq G_\delta(0)$, to eliminate the inevitable steady-state error, an additional feed-forward control input can be designed following the ideas given in Garcia and Morari (1982) and Morari and Zafiriou (1989).

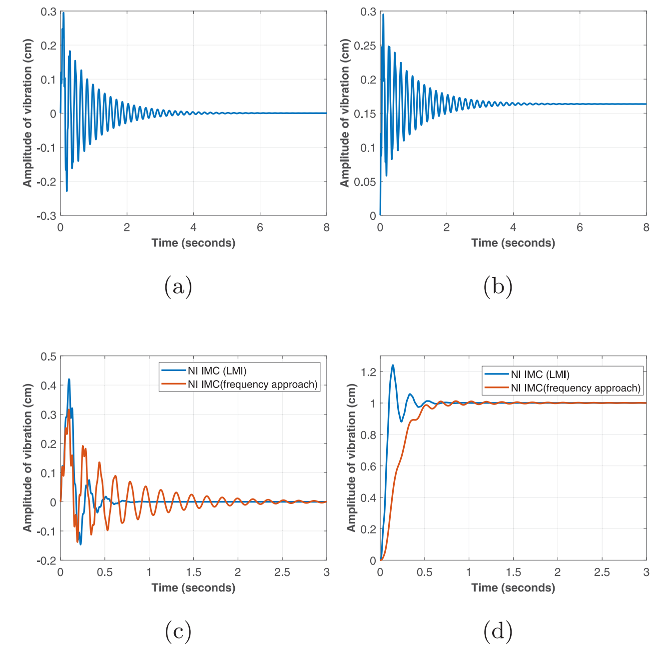

Fig. 12. [When $G(s) \neq G_m(s)$] (a) Open-loop response to a pulse input; (b) Open-loop response to a unit step input; (c) Closed-loop pulse response using the controllers $C_1(s)$ [via frequency-domain approach] and $C_2(s)$ [via the LMI-based approach]; (d) Closed-loop unit step response using the controllers $C_1(s)$ and $C_2(s)$.

4.4. Experimental validation results

This subsection will test the feasibility and performance of the NI-based IMC controller $C_2(s)$ given in (16) on a vibration control problem of a lightweight cantilever beam. A custom-made vibration suppressor shown in Fig. 3 was considered for the experimental validation purposes. The complete closed-loop control setup is shown in Fig. 9(a). The cantilever beam we considered for experimental validation has a SISO configuration, that is, a single pair of collocated force actuator and position sensor. Both the sensor and actuator use MFC patches glued with the beam.

4.4.1. Regulatory response (disturbance rejection performance) under nominal condition

The regulatory response (under a nominal operating condition) of the vibration suppressor system was tested by shaking the base unit (which acts as a disturbance) of the system through the belt–pulley–motor arrangement. A PWM signal was applied

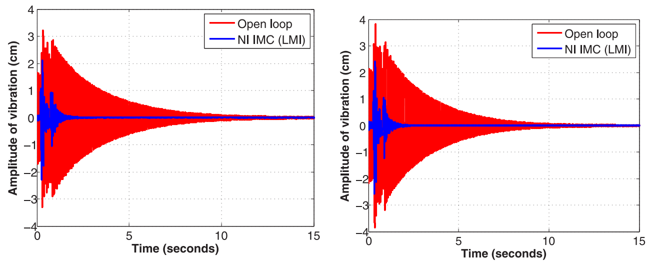

(a) (b)

Fig. 13. [Experimental validation results: Regulatory response achieved by $C_2(s)$] (a) under nominal operating condition; and (b) when an external weight was attached to the beam.

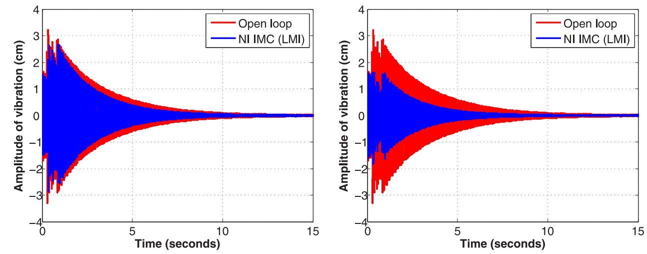

(a) (b)

Fig. 14. Experimental validation results — Regulatory responses (Disturbance rejection capability) achieved by the new IMC controllers: (a) $C_3(s)$ and (b) $C_4(s)$.

to the input of the motor for a duration of 0.5 s to produce a jerk that induces a vibration in the beam. The disturbance rejection performance is evident from Fig. 13(a), which reveals that the controller $C_2(s)$ has significantly attenuated the vibration caused by the external disturbance produced by the belt–pulley–motor assembly. The figure also compares the regulatory response with the open-loop response subject to the disturbance. The regulatory response has a decay time of 2.17 s and a peak overshoot of 2.036 cm compared to the open-loop response having a decay time of 11.50 s and a peak overshoot of 3.2190 cm. Please access the following web links https://youtu.be/CljRUaelS6Q and https://youtu.be/io4a4JXfFDI to watch the experimental demonstration clips.

4.4.2. Regulatory response (disturbance rejection) under perturbed condition

To test the robustness of the proposed NI-based IMC scheme against a deliberate model mismatch [i.e. when $G(s)$ is significantly different from the $G_m(s)$], we attached an external weight of 5 g mass to the existing beam at the middle position. The beam has a mass of 30 g, making the total mass of the beam and weight 35 g. This hardware change shifts the unperturbed resonant modes of the beam. Then, the same experiment as done in Section 4.4.1 was carried out. Fig. 13(b) shows the disturbance rejection capability of $C_2(s)$ in the perturbed situation. It can be noticed that the controller produces satisfactory performance even in this case also.

4.4.3. Effect of changes in $d(s)$ on the transient performance of the controller

This subsection analyses the effect of changing the real root of the polynomial $d(s) = (s + a)\mathbb{D}\big[G_m(s)\big]$ on the closed-loop performance tested in experimentation. We took two different choices $a_1 = 0.8$ and $a_2 = 8$, fixed respectively at two decades and one decade below the first resonant mode (at $\omega = 80$ rad/s) of the identified plant model $G_m(s)$. We seek to redesign the IMC controller via the LMI-based design methodology (i.e. Theorem 2) corresponding to the two new polynomials $d_2(s) = (s + 0.8)\mathbb{D}\big[G_m(s)\big]$ and $d_3(s) = (s+8)\mathbb{D}\big[G_m(s)\big]$. The new controllers are obtained as:

$$C_3(s) = \frac{5.9357(s + 0.8385)}{(s + 0.8)(s + 2.033)} \tag{18}$$

and

$$C_4(s) = \frac{10.941(s + 12.56)}{(s + 8)(s + 5.615)}. \tag{19}$$

Note that $C_3(s)$ and $C_4(s)$ contain slower poles than $C_2(s)$, which have been dictated by the factors $(s + 0.8)$ in $d_2(s)$ and $(s + 8)$ in $d_3(s)$, respectively. The closed-loop stability of the IMC scheme is still guaranteed since both $C_3(s)$ and $C_4(s)$ satisfy the DC loop gain condition, as verified here: $C_3(0)G_m(0) = 3.0592 \times 0.1618 = 0.4950 < 1$ and $C_4(0)G_m(0) = 3.0596 \times 0.1618 = 0.4951 < 1$.

Figs. 14(a) and 14(b) portray the regulatory responses (which reflects the disturbance rejection capability) achieved by the new controllers $C_3(s)$ and $C_4(s)$. Comparing Figs. 14(a), 14(b) and 13(a), it can be asserted that $C_2(s)$ offers the best vibration attenuation performance. The decay time (considering a 2% tolerance band) in case of $C_2(s)$ is even smaller than 2 s, in contrast to 8.5 s achieved by $C_3(s)$ and 4 s achieved by $C_4(s)$ respectively. Therefore, we conjecture that as the real root (at $s = -a$) of $d(s)$ moves farther in the left-hand side of the s-plane, the speed of response improves. Regarding the vibration-amplitude reduction, $C_4(s)$ and $C_2(s)$ reduce the open-loop peak vibration of 3.2 cm to 1.95 cm (shown in Fig. 14(b)) and 2.095 cm (shown in Fig. 13(a)) respectively. However, the degree of vibration attenuation in the case of $C_3(s)$ is much less than that achieved by $C_2(s)$ and $C_4(s)$. The experimental results suggest that the real root (at $s = -a$) of $d(s)$ should not be placed more than a decade below the first resonant mode of the plant model $G_m(s)$.

5. Conclusions

This paper has introduced a Negative Imaginary (NI) controller synthesis technique based on a positive feedback Internal Model Control framework (see Fig. 4). A frequency-domain and an LMI-based design methodology are proposed for generating the NI controller. The frequency-domain design technique offers two specific controller forms and solves a constrained least-square estimation problem to find the controller parameters. While the LMI-based methodology relies on the choice of a stable polynomial $d(s)$, which plays a crucial role in constructing the auxiliary filter $F(s) = G_m(s)Q(s)$ that governs the shape of the closed-loop time response. A systematic set of guidelines is provided for choosing the polynomial $d(s)$. Both synthesis techniques ensure closed-loop stability, even in the presence of model-mismatch, and achieve perfect steady-state tracking. Simulation studies accompanied by experimental results are given, which advocate the feasibility and effectiveness of the proposed NI-based IMC scheme in the vibration attenuation of a lightweight cantilever beam.

Acknowledgements

The authors express their sincere thanks to the Associate Editor and the anonymous reviewers for giving constructive comments and useful suggestions that have really helped to improve the quality and clarity of the paper.

Appendix

Let $\Gamma(s, z_i) = (s + z_i)(s + \bar{z}_i)$.

Table 1
Quantitative information of the performance parameters of the closed-loop impulse response of the plant model G_{m_1} subject to the choice of the pole polynomials $\{d_1(s),\ d_2(s),\ \ldots,\ d_{30}(s)\}$.

Choice of $d(s)$	Bandwidth	Impulse response settling time	Peak of impulse response	Farthest controller pole
$d_1(s) = (s+0.5)\Gamma(s, 0.5+j)$	1.018	26.474	0.484	−5.911
$d_2(s) = (s+0.5)\Gamma(s, 0.5+2j)$	1.052	35.207	0.545	−34.710
$d_3(s) = (s+0.5)\Gamma(s, 0.5+3j)$	0.964	38.718	0.499	−32.533
$d_4(s) = (s+0.5)\Gamma(s, 0.5+4j)$	0.981	38.272	0.512	−39.526
$d_5(s) = (s+1)\Gamma(s, 1+j)$	1.051	34.994	0.538	−36.433
$d_6(s) = (s+1)\Gamma(s, 1+2j)$	0.991	37.108	0.511	−34.295
$d_7(s) = (s+1)\Gamma(s, 1+3j)$	0.858	43.075	0.440	−56.949
$d_8(s) = (s+1)\Gamma(s, 1+4j)$	0.883	42.331	0.461	−63.009
$d_9(s) = (s+2)\Gamma(s, 2+j)$	0.448	42.349	0.484	−75.035
$d_{10}(s) = (s+2)\Gamma(s, 2+2j)$	0.881	42.153	0.455	−77.485
$d_{11}(s) = (s+2)\Gamma(s, 2+3j)$	0.891	41.910	0.463	−81.548
$d_{12}(s) = (s+2)\Gamma(s, 2+4j)$	0.776	47.642	0.400	−152.346
$d_{13}(s) = (s+3)\Gamma(s, 3+j)$	0.888	42.220	0.463	−112.141
$d_{14}(s) = (s+3)\Gamma(s, 3+2j)$	0.717	45.156	0.363	−225.809
$d_{15}(s) = (s+3)\Gamma(s, 3+3j)$	0.847	44.215	0.442	−156.8465
$d_{16}(s) = (s+3)\Gamma(s, 3+4j)$	0.574	48.655	0.286	−458.572
$d_{17}(s) = (s+4)\Gamma(s, 4+j)$	0.569	49.046	0.283	−523.863
$d_{18}(s) = (s+4)\Gamma(s, 4+2j)$	0.559	49.712	0.278	−569.341
$d_{19}(s) = (s+4)\Gamma(s, 4+3j)$	0.534	51.637	0.262	−683.768
$d_{20}(s) = (s+4)\Gamma(s, 4+4j)$	0.535	51.756	0.263	−691.803
$d_{21}(s) = (s+5)\Gamma(s, 5+j)$	0.597	53.713	0.301	−617.6388
$d_{22}(s) = (s+5)\Gamma(s, 5+2j)$	0.606	53.183	0.307	−597.666
$d_{23}(s) = (s+5)\Gamma(s, 5+3j)$	0.618	52.458	0.313	−576.443
$d_{24}(s) = (s+5)\Gamma(s, 5+4j)$	0.605	53.389	0.306	−599.979
$d_{25}(s) = (s+1)\mathbb{D}\left[G_m(s)\right]$	1.054	24.714	0.491	−15.136
$d_{26}(s) = (s+1)^3$	0.997	27.596	0.486	−7.511
$d_{27}(s) = (s+0.5)^3$	1.048	29.637	0.488	−9.414
$d_{28}(s) = (s+2)^3$	0.865	42.384	0.445	−74.781
$d_{29}(s) = (s+3)^3$	0.877	42.664	0.457	−114.690
$d_{30}(s) = (s+4)^3$	0.858	43.775	0.449	−185.911

Table 2
Quantitative information of the performance parameters of the closed-loop impulse response of the plant model G_{m_2} subject to the choice of the pole polynomials $\{d_1(s),\ d_2(s),\ \ldots,\ d_{30}(s)\}$.

Choices of $d(s)$	Bandwidth	Impulse response settling time	Peak of impulse response	Farthest controller pole
$d_1(s) = (s+15)\Gamma(s, 15+j)$	0.087	37.684	0.162	−15
$d_2(s) = (s+15)\Gamma(s, 15+2j)$	0.087	37.641	0.162	−15
$d_3(s) = (s+15)\Gamma(s, 15+3j)$	0.088	37.573	0.163	−15
$d_4(s) = (s+15)\Gamma(s, 15+4j)$	0.088	37.473	0.163	−15
$d_5(s) = (s+16)\Gamma(s, 16+j)$	0.162	20.262	0.304	−16
$d_6(s) = (s+16)\Gamma(s, 16+2j)$	0.162	20.252	0.304	−16
$d_7(s) = (s+16)\Gamma(s, 16+3j)$	0.162	20.240	0.304	−16
$d_8(s) = (s+16)\Gamma(s, 16+4j)$	0.162	20.220	0.304	−16
$d_9(s) = (s+17)\Gamma(s, 17+j)$	0.171	19.200	0.320	−17
$d_{10}(s) = (s+17)\Gamma(s, 17+2j)$	0.171	19.186	0.321	−17
$d_{11}(s) = (s+17)\Gamma(s, 17+3j)$	0.171	19.164	0.321	−17
$d_{12}(s) = (s+17)\Gamma(s, 17+4j)$	0.171	19.130	0.322	−17
$d_{13}(s) = (s+18)\Gamma(s, 18+j)$	0.181	18.114	0.340	−18
$d_{14}(s) = (s+18)\Gamma(s, 18+2j)$	0.181	18.101	0.340	−18
$d_{15}(s) = (s+18)\Gamma(s, 18+3j)$	0.181	18.077	0.340	−18
$d_{16}(s) = (s+18)\Gamma(s, 18+4j)$	0.182	18.042	0.341	−18
$d_{17}(s) = (s+19)\Gamma(s, 19+j)$	0.177	18.558	0.332	−19
$d_{18}(s) = (s+19)\Gamma(s, 19+2j)$	0.177	18.553	0.332	−19
$d_{19}(s) = (s+19)\Gamma(s, 19+3j)$	0.177	18.541	0.332	−19
$d_{20}(s) = (s+19)\Gamma(s, 19+4j)$	0.177	18.525	0.332	−19
$d_{21}(s) = (s+20)\Gamma(s, 20+j)$	0.190	17.223	0.357	−20
$d_{22}(s) = (s+20)\Gamma(s, 20+2j)$	0.190	17.224	0.357	−20
$d_{23}(s) = (s+20)\Gamma(s, 20+3j)$	0.190	17.224	0.357	−20
$d_{24}(s) = (s+20)\Gamma(s, 20+4j)$	0.190	17.223	0.357	−20
$d_{25}(s) = (s+19)\mathbb{D}\left[G_m(s)\right]$	1.671	5.585	2.372	−19
$d_{26}(s) = (s+15)^3$	0.087	37.689	0.162	−15
$d_{27}(s) = (s+16)^3$	0.162	20.261	0.304	−16
$d_{28}(s) = (s+17)^3$	0.171	19.204	0.320	−17
$d_{29}(s) = (s+18)^3$	0.181	18.119	0.340	−18
$d_{30}(s) = (s+19)^3$	0.177	18.561	0.332	−19

Table 3
Quantitative information of the performance parameters of the closed-loop impulse response of the plant model G_{m_3} subject to the choice of the pole polynomials $\{d_1(s),\ d_2(s),\ \ldots,\ d_{30}(s)\}$.

Choices of $d(s)$	Bandwidth	Impulse settling time	Peak of impulse response	Farthest controller pole
$d_1(s) = (s+0.5)\Gamma(s, 0.5+j)$	0.187	21.613	0.180	−0.500
$d_2(s) = (s+0.5)\Gamma(s, 0.5+2j)$	1.113	9.935	0.438	−2.204
$d_3(s) = (s+0.5)\Gamma(s, 0.5+3j)$	0.933	10.962	0.378	−2.788
$d_4(s) = (s+0.5)\Gamma(s, 0.5+4j)$	0.994	11.247	0.399	−3.160
$d_5(s) = (s+1)\Gamma(s, 1+j)$	1.258	11.625	0.547	−2.398
$d_6(s) = (s+1)\Gamma(s, 1+2j)$	0.938	10.981	0.380	−2.875
$d_7(s) = (s+1)\Gamma(s, 1+3j)$	0.819	15.026	0.387	−4.3269
$d_8(s) = (s+1)\Gamma(s, 1+4j)$	1.013	25.767	0.535	−13.631
$d_9(s) = (s+2)\Gamma(s, 2+j)$	1.035	24.387	0.533	−14.170
$d_{10}(s) = (s+2)\Gamma(s, 2+2j)$	1.051	24.261	0.539	−14.418
$d_{11}(s) = (s+2)\Gamma(s, 2+3j)$	1.000	31.285	0.559	−19.215
$d_{12}(s) = (s+2)\Gamma(s, 2+4j)$	0.948	31.772	0.559	−21.571
$d_{13}(s) = (s+3)\Gamma(s, 3+j)$	0.971	31.574	0.572	−23.823
$d_{14}(s) = (s+3)\Gamma(s, 3+2j)$	0.711	37.441	0.412	−49.524
$d_{15}(s) = (s+3)\Gamma(s, 3+3j)$	0.703	44.379	0.424	−58.237
$d_{16}(s) = (s+3)\Gamma(s, 3+4j)$	0.720	43.426	0.438	−58.267
$d_{17}(s) = (s+4)\Gamma(s, 4+j)$	0.753	41.711	0.462	−60.540
$d_{18}(s) = (s+4)\Gamma(s, 4+2j)$	0.750	42.160	0.461	−61.670
$d_{19}(s) = (s+4)\Gamma(s, 4+3j)$	0.765	41.233	0.472	−60.913
$d_{20}(s) = (s+4)\Gamma(s, 4+4j)$	0.798	44.505	0.499	−62.081
$d_{21}(s) = (s+5)\Gamma(s, 5+j)$	0.736	49.277	0.470	−148.413
$d_{22}(s) = (s+5)\Gamma(s, 5+2j)$	0.742	48.953	0.475	−147.945
$d_{23}(s) = (s+5)\Gamma(s, 5+3j)$	0.754	47.966	0.484	−146.765
$d_{24}(s) = (s+5)\Gamma(s, 5+4j)$	0.640	49.269	0.381	−174.383
$d_{25}(s) = (s+1.41)\mathbb{D}\big[G_m(s)\big]$	1.445	20.512	0.846	−15.706
$d_{26}(s) = (s+1.41)^3$	0.955	11.146	0.384	−3.056
$d_{27}(s) = (s+3)\mathbb{D}\big[G_m(s)\big]$	1.445	16.041	0.839	−32.709
$d_{28}(s) = (s+3)^3$	0.974	31.521	0.572	−23.508
$d_{29}(s) = (s+1.41)^2(s+3)$	0.995	11.387	0.398	−3.458
$d_{30}(s) = (s+1.41)(s+3)^2$	1.062	27.553	0.547	−15.706

Table 4
Quantitative information of the performance parameters of the closed-loop impulse response of the plant model G_{m_4} subject to the choice of the pole polynomials $\{d_1(s),\ d_2(s),\ \ldots,\ d_{30}(s)\}$.

Choices of $d(s)$	Bandwidth	Impulse response settling time	Peak of impulse response	Farthest controller pole
$d_1(s) = (s+0.5)\Gamma(s, 0.5+j)$	1.197	15.725	0.438	−7.769
$d_2(s) = (s+0.5)\Gamma(s, 0.5+2j)$	0.745	16.0688	0.330	−15.272
$d_3(s) = (s+0.5)\Gamma(s, 0.5+3j)$	0.899	25.163	0.427	−30.813
$d_4(s) = (s+0.5)\Gamma(s, 0.5+4j)$	0.906	30.061	0.450	−40.171
$d_5(s) = (s+1)\Gamma(s, 1+j)$	0.921	15.558	0.390	−12.305
$d_6(s) = (s+1)\Gamma(s, 1+2j)$	0.573	21.040	0.255	−23.090
$d_7(s) = (s+1)\Gamma(s, 1+3j)$	0.856	26.372	0.405	−34.181
$d_8(s) = (s+1)\Gamma(s, 1+4j)$	0.518	41.412	0.242	−97.868
$d_9(s) = (s+2)\Gamma(s, 2+j)$	0.755	24.216	0.358	−54.891
$d_{10}(s) = (s+2)\Gamma(s, 2+2j)$	0.636	28.746	0.300	−88.390
$d_{11}(s) = (s+2)\Gamma(s, 2+3j)$	0.587	36.184	0.271	−87.837
$d_{12}(s) = (s+2)\Gamma(s, 2+4j)$	0.582	39.256	0.281	−104.549
$d_{13}(s) = (s+3)\Gamma(s, 3+j)$	0.642	34.516	0.295	−86.870
$d_{14}(s) = (s+3)\Gamma(s, 3+2j)$	0.617	42.560	0.295	−115.381
$d_{15}(s) = (s+3)\Gamma(s, 3+3j)$	0.483	45.954	0.239	−180.854
$d_{16}(s) = (s+3)\Gamma(s, 3+4j)$	0.476	47.855	0.248	−190.276
$d_{17}(s) = (s+4)\Gamma(s, 4+j)$	0.485	45.965	0.240	−199.757
$d_{18}(s) = (s+4)\Gamma(s, 4+2j)$	0.428	51.235	0.207	−347.180
$d_{19}(s) = (s+4)\Gamma(s, 4+3j)$	0.386	46.667	0.181	−404.683
$d_{20}(s) = (s+4)\Gamma(s, 4+4j)$	0.261	48.585	0.112	−779.683
$d_{21}(s) = (s+5)\Gamma(s, 5+j)$	0.306	53.346	0.134	−685.419
$d_{22}(s) = (s+5)\Gamma(s, 5+2j)$	0.424	63.030	0.217	−729.551
$d_{23}(s) = (s+5)\Gamma(s, 5+3j)$	0.437	61.940	0.226	−714.432
$d_{24}(s) = (s+5)\Gamma(s, 5+4j)$	0.377	59.740	0.183	−739.188
$d_{25}(s) = (s+1.37)\mathbb{D}\big[G_m(s)\big]$	1.418	20.982	0.998	−30.837
$d_{26}(s) = (s+1.37)^3$	0.645	15.785	0.289	−14.587
$d_{27}(s) = (s+2.93)\mathbb{D}\big[G_m(s)\big]$	1.445	16.041	0.839	−32.709
$d_{28}(s) = (s+2.93)^3$	0.523	33.702	0.238	−119.702
$d_{29}(s) = (s+3.6)\mathbb{D}\big[G_m(s)\big]$	1.430	20.048	1.101	−83.771
$d_{30}(s) = (s+3.6)^3$	0.501	44.872	0.250	−181.865

References

Angeli, D. (2006). Systems with counterclockwise input-output dynamics. *IEEE Transactions on Automatic Control*, *51*(7), 1130–1143.

Bhowmick, P., & Lanzon, A. (2019). Output strictly negative imaginary systems and its connections to dissipativity theory. In *Proceedings of 58th IEEE conference on decision and control* (pp. 6754–6759).

Bhowmick, P., & Lanzon, A. (2020). Time-domain output negative imaginary systems and its connection to dynamic dissipativity. In *Proceedings of 59th IEEE conference on decision and control* (pp. 5167–5172).

Bhowmick, P., & Lanzon, A. (2024). Dynamic dissipative characterisation of time-domain input-output negative imaginary systems. *Automatica*, 1–14, in press.

Bhowmick, P., & Patra, S. (2017). On LTI output strictly negative-imaginary systems. *Systems & Control Letters*, *100*, 32–42.
Bhowmick, P., & Patra, S. (2020). Solution to negative-imaginary control problem for uncertain LTI systems with multi-objective performance. *Automatica*, *112*(108735), 1–9.
Boyd, S., El Ghaoui, L., Feron, E., & Balakrishnan, V. (1994). *Studies in applied mathematics*: *vol. 15*, *Linear matrix inequalities in system and control theory*. Philadelphia, PA: SIAM.
Dey, A., Patra, S., & Sen, S. (2019). Stability analysis and controller design for Luré system with hysteresis nonlinearities: A negative-imaginary theory based approach. *International Journal of Control*, *92*(8), 1903–1913.
Ferrante, A., Lanzon, A., & Ntogramatzidis, L. (2016). Foundations of not necessarily rational negative imaginary systems theory: Relations between classes of negative imaginary and positive real systems. *IEEE Transactions on Automatic Control*, *61*(10), 3052–3057.
Ferrante, A., Lanzon, A., & Ntogramatzidis, L. (2017). Discrete-time negative imaginary systems. *Automatica*, *79*, 1–10.
Ferrante, A., & Ntogramatzidis, L. (2013). Some new results in the theory of negative imaginary systems with symmetric transfer matrix function. *Automatica*, *49*(7), 2138–2144.
Garcia, C. E., & Morari, M. (1982). Internal model control: A unifying review and some new results. *Industrial and Engineering Chemistry Process Design and Development*, *21*(2), 308–323.
Grant, M., & Boyd, S. (2014). CVX: Matlab software for disciplined convex programming, version 2.1. http://cvxr.com/cvx.
Hu, J., Lennox, B., & Arvin, F. (2022). Robust formation control for networked robotic systems using negative imaginary dynamics. *Automatica*, *140*(110235), 1–9.
Kurawa, S., Bhowmick, P., & Lanzon, A. (2019). Dynamic output feedback controller synthesis using an LMI-based α-strictly negative imaginary framework. In *Proceedings of 27th mediterranean conference on control and automation* (pp. 81–86).
Lanzon, A., & Bhowmick, P. (2023). Characterisation of input-output negative imaginary systems in a dissipative framework. *IEEE Transactions on Automatic Control*, *68*(2), 959–974.
Lanzon, A., & Chen, H.-J. (2017). Feedback stability of negative imaginary systems. *IEEE Transactions on Automatic Control*, *62*(11), 5620–5633.
Lanzon, A., & Petersen, I. R. (2008). Stability robustness of a feedback interconnection of systems with negative imaginary frequency response. *IEEE Transactions on Automatic Control*, *53*(4), 1042–1046.
Lanzon, A., Song, Z., Patra, S., & Petersen, I. R. (2011). A strongly strict negative-imaginary lemma for non-minimal linear systems. *Communications in Information and Systems*, *11*(2), 139–152.
Li, C., Wang, J., Shan, J., Lanzon, A., & Petersen, I. R. (2021). Robust cooperative control of networked train platoons: A negative-imaginary systems' perspective. *IEEE Transactions on Control of Network Systems*, *8*(4), 1743–1753.
Liu, K.-Z., Ono, M., Li, X., & Wu, M. (2017). Robust performance synthesis for systems with positive-real uncertainty and an extension to the negative-imaginary case. *Automatica*, *82*, 194–201.
Liu, M., & Xiong, J. (2017). Properties and stability analysis of discrete-time negative imaginary systems. *Automatica*, *83*, 58–64.
Mabrok, M. A., Kallapur, A. G., Petersen, I. R., & Lanzon, A. (2014). Generalizing negative imaginary systems theory to include free body dynamics: Control of highly resonant structures with free body motion. *IEEE Transactions on Automatic Control*, *59*(10), 2692–2707.
Morari, M., & Zafiriou, E. (1989). *Robust process control* (1st ed.). Englewood Cliffs, New Jersey, USA: Prentice Hall.
Nikooienejad, N., & Reza Moheimani, S. O. (2022). Convex synthesis of SNI controllers based on frequency-domain data: MEMS nanopositioner example. *IEEE Transactions on Control Systems Technology*, *30*(2), 767–778.
Petersen, I. R. (2016). Negative imaginary systems theory and applications. *Annual Reviews in Control*, *42*, 309–318.
Scherer, C., Gahinet, P., & Chilali, M. (1997). Multi objective output-feedback control via LMI optimization. *IEEE Transactions on Automatic Control*, *42*(7), 896–911.
Shi, K., Petersen, I. R., & Vladimirov, I. G. (2023). Output feedback consensus for networked heterogeneous nonlinear negative-imaginary systems with free-body motion. *IEEE Transactions on Automatic Control*, *68*(9), 5536–5543.
Song, Z., Lanzon, A., Patra, S., & Petersen, I. R. (2010). Towards controller synthesis for systems with negative imaginary frequency response. *IEEE Transactions on Automatic Control*, *55*(6), 1506–1511.
Song, Z., Lanzon, A., Patra, S., & Petersen, I. R. (2012a). A negative-imaginary lemma without minimality assumptions and robust state-feedback synthesis for uncertain negative-imaginary systems. *Systems & Control Letters*, *61*(12), 1269–1276.
Song, Z., Lanzon, A., Patra, S., & Petersen, I. R. (2012b). Robust performance analysis for uncertain negative-imaginary systems. *International Journal of Robust and Nonlinear Control*, *22*(3), 262–281.
Su, Y., Bhowmick, P., & Lanzon, A. (2023a). Cooperative control of multi-agent negative imaginary systems with applications to UAVs, including hardware implementation results. In *Proceedings of the 2023 European control conference* (pp. 1979–1984).
Su, Y., Bhowmick, P., & Lanzon, A. (2023b). A negative imaginary theory-based time-varying group formation tracking scheme for multi-robot systems: Applications to quadcopters. In *Proceedings of the 2023 IEEE international conference on robotics and automation* (pp. 1435–1441).
Su, Y., Bhowmick, P., & Lanzon, A. (2023c). Properties of interconnected negative imaginary systems and extension to formation-containment control of networked multi-UAV systems with experimental validation results. *Asian Journal of Control*, 1–18.
Tran, V. P., Garratt, M. A., & Petersen, I. R. (2021). Multi-vehicle formation control and obstacle avoidance using negative-imaginary systems theory. *IFAC Journal of Systems and Control*, *15*(100117), 1–23.
Xiong, J., Lam, J., & Petersen, I. R. (2016). Output feedback negative imaginary synthesis under structural constraints. *Automatica*, *71*, 222–228.
Xiong, J., Petersen, I. R., & Lanzon, A. (2010). A negative imaginary lemma and the stability of interconnections of linear negative imaginary systems. *IEEE Transactions on Automatic Control*, *55*(10), 2342–2347.

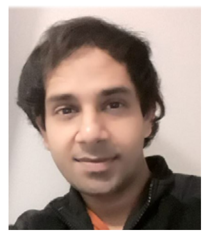

Parijat Bhowmick is presently an Assistant Professor at the Dept. of EEE of IIT Guwahati, India. Before joining this position, he worked for three years as a Post-doctoral Research Associate at the Control Systems Centre, University of Manchester. He completed his Ph.D. in Control Engineering from IIT Kharagpur, India, in 2018. He did his Master's from Jadavpur University in 2012 with the same specialisation. He received the University Gold Medal in his Masters and the Institute Silver Medal during his Bachelor's. He is an active researcher in the horizon of Robust control of uncertain systems, Negative Imaginary Systems theory, Vibration control of mechatronic systems, Cooperative Control of Multi-agent Systems (including multi-agent Systems) and Control of Smart/Micro-grid Systems.

Suleiman Kurawa received his undergraduate degree (First class) from Bayero University, Kano, in 2011. He also received an M.Sc. in Advanced Control and System Engineering (Distinction) and a Ph.D. in Electrical and Electronic Engineering from the University of Manchester in 2014 and 2020, respectively. He has received many awards and scholarships, including the best graduating undergraduate student in the Faculty of Engineering, the National Information Technology Development Agency (NITDA) scholarship, and the Petroleum Trust Development Fund (PTDF) scholarship. His research interest is in robust control and dissipative systems, emphasising Negative Imaginary theory and its application to vibration attenuation in flexible structures. He is currently with RollsRoyce Plc as a System Design Engineer.

Somasundar Kannan received his B.Eng. degree in Electronics and Instrumentation from the University of Madras, India; MS degree in Aerospace Engineering from Korea Advanced Institute of Science and Technology (KAIST), Republic of Korea and Ph.D. in Automatic Control from Arts et Métiers Institute of Technology, France. He is currently a Lecturer in Electronic and Electrical Engineering at Robert Gordon University (RGU), UK. Previously, he worked as a research engineer and postdoctoral researcher at Centrale Supeléc, France, University of Luxembourg, Luxembourg, and University of Manchester, UK. His research interests include Model Predictive Control, Nonlinear and Adaptive Control, and Cooperative and Distributed control.

Alexander Lanzon received his Ph.D. degree in Control Engineering and his M.Phil. degree in Robot Control from the University of Cambridge, Cambridge, UK, in 2000 and 1997 respectively and received his B.Eng. (Hons.) degree in Electrical and Electronic Engineering from the University of Malta, Msida, Malta, in 1995.

He has held research and academic positions at Georgia Institute of Technology, Atlanta GA, USA, and the Australian National University, Canberra ACT, Australia, and industrial positions at ST-Microelectronics

Ltd., Kirkop, Malta; Yaskawa Denki (Tokyo) Ltd., SaitamaKen, Japan; and National ICT Australia Ltd., Canberra ACT, Australia. In 2006, he joined the University of Manchester, Manchester, UK, where he now holds the Chair in Control Engineering. His research interests include the fundamentals of feedback control theory, negative imaginary systems theory, robust control theory, input–output nonlinear control theory, and applying robust and nonlinear control theory to innovative mechatronic, robotic and drone applications.

Prof. Lanzon is a Fellow of the Institute of Mathematics and its Applications, the Institute of Measurement and Control and the Institution of Engineering and Technology. He is currently an Associate Editor of the IEEE Control Systems Letters (L-CSS). He has served as an Associate Editor of the IEEE Transactions on Automatic Control from 2012 to 2018, and as a Subject Editor of the International Journal of Robust and Nonlinear Control from 2012 to 2015.